The Meteoritical Society

Meteoritics & Planetary Science 42, Nr 7/8, 1077–1101 (2007)
Abstract available online at http://meteoritics.org

NanoSIMS studies of Ba isotopic compositions in single presolar silicon carbide grains from AGB stars and supernovae

K. K. MARHAS[†*], P. HOPPE, and U. OTT

Max-Planck-Institut für Chemie, P.O. Box 3060, 55020 Mainz, Germany
[†]Present address: Kuljeet Kaur Marhas, Physical Research Laboratory, Navrangpura, Ahmedabad 380009, India
[*]Corresponding author. E-mail: kkmarhas@prl.res.in

(Received 13 September 2006; revision accepted 29 April 2007)

Abstract–We have studied 74 single presolar silicon carbide grains with sizes between 0.2 and 2.6 μm from the Murchison and Murray meteorites for Ba isotopic compositions using NanoSIMS. We also analyzed 7 SiC particles either consisting of sub-micron-size SiC grains or representing a morphologically and isotopically distinct subgroup. Of the 55 (likely) mainstream grains, originating from asymptotic giant branch (AGB) stars, 32 had high enough Ba contents for isotopic analysis. For 26 of them, CsH_x interferences were either negligible or could be corrected with confidence. They exhibit typical *s*-process Ba isotopic patterns with slightly higher than solar $^{134}Ba/^{136}Ba$ and lower than solar $^{135,137,138}Ba/^{136}Ba$ ratios. Results are generally well explained in the context of neutron capture nucleosynthesis in low mass (1–3 $M_\odot$) AGB stars and provide constraints on AGB models, by reducing the needed ^{13}C spread from factor of ~20 down to 2. Out of the 19 supernova X grains, three had sufficient concentrations for isotopic analysis. They tend to exhibit higher than solar $^{134}Ba/^{136}Ba$ and $^{138}Ba/^{136}Ba$ ratios, close to solar $^{137}Ba/^{136}Ba$, and $^{135}Ba/^{136}Ba$ lower than solar but higher than in mainstream grains. This signature could indicate a mixture of n-burst type Ba with either "normal Ba" more *s*-process-rich than solar, or normal Ba plus weak *s*-process Ba. In the n-burst component Cs may have to be separated from Ba at ~10 years after the SN explosion. Depending on predictions for its composition, another possibility is early separation (at ~1 year) coupled with addition of some unfractionated n-burst matter. Abundances of trace elements (Sr, Zr, Cs, La, and Ce) analyzed along with Ba signify that implantation may have been an important process for their introduction.

INTRODUCTION

The nuclear processes responsible for the production of the heavy elements and isotopes in stars are mainly associated with the capture of neutrons. Two different modes of neutron capture reactions identified/distinguished on the basis of different time scales for the capture of neutrons are the s-process (slow) and the *r*-process (rapid) (Burbidge et al. 1957). In the *s*-process, n-capture occurs on a time scale much longer than the beta decay times of the newly formed isotopes; the *r*-process shows just the opposite characteristics. The first experimental evidence for isotope abundance anomalies in the heavy elements possibly associated with these processes was seen in the Xe isotopic signature of the CR2 chondrite Renazzo (Reynolds and Turner 1964). The anomaly now generally referred to as Xe-HL (e.g., Huss and Lewis 1994) was discussed in terms of nuclear processes (*r*- and *s*-) based on larger effects seen in the Allende CV3 chondrite (Manuel et al. 1972). A milestone in the search for the carriers of anomalies in Xe (and other noble gases) was the realization by Lewis et al. (1975) that they were resistant to acids, which later allowed their isolation and identification as presolar grains of circumstellar origin: nanodiamonds as carriers of the Xe-HL anomaly (Lewis et al. 1987) and silicon carbide (SiC) as the host phase of Xe showing the signature of the *s*-process and also carrying nearly mono-isotopic ^{22}Ne (Bernatowicz et al. 1987). An additional production mechanism for some heavy nuclides is by capture of protons, the so-called *p*-process.

Circumstellar grains condense in the winds or ejecta of evolved stars, thereby acquiring the characteristic isotopic compositions of the parent stars. Presolar grains identified by now include, besides diamond and silicon carbide, graphite, silicon nitride (Si_3N_4), corundum (Al_2O_3), spinel ($MgAl_2O_4$),

hibonite ($CaAl_{12}O_{19}$), titanium oxide (TiO_2) (Zinner 2004; Hoppe 2004; Nittler 2003), and the recently discovered silicates (Messenger et al. 2003; Nguyen and Zinner 2004; Mostefaoui and Hoppe 2004).

The most extensively studied presolar mineral is SiC. Reasons for this are its relatively high abundance (several ppm) in primitive meteorites, the possibility to produce almost pure SiC separates by physical and chemical treatments, and the large size (>1 μm) of many grains. Based on the isotopic compositions of C, N, and Si, SiC was divided into six distinct groups: mainstream, X, Y, Z, A, and B (Hoppe and Ott 1997). Around ninety percent of the SiC grains are of the mainstream type, with $^{12}C/^{13}C$ ratios of 10–100, $^{14}N/^{15}N$ ratios between 50 and 19,000, and Si isotopic compositions which plot on a slope 1.34 line in a three isotope $\delta^{29}Si/^{28}Si$ versus $\delta^{30}Si/^{28}Si$ representation (δ is the deviation in permil with regard to solar values). The mainstream grains are believed to have formed in the winds of thermally pulsing low-mass (1–3 $M_\odot$) asymptotic giant branch (AGB) stars (Gallino et al. 1993, 1998; Hoppe and Ott 1997; Lugaro et al. 2003). Type X grains constitute only about one percent of the total population of the SiC grains and are characterized by enrichments in ^{28}Si ($^{29,30}Si/^{28}Si$ significantly lower than solar), isotopically heavy nitrogen ($^{14}N/^{15}N < 272$), isotopically light carbon ($^{12}C/^{13}C > 89$) in most grains, high abundances of now extinct ^{26}Al at the time of grain formation ($[^{26}Al/^{27}Al]_{ini} > 0.01$), and in some grains presence of the decay products of now extinct ^{44}Ti and ^{49}V. These characteristics point toward formation from the ejecta of type II supernovae (Amari et al. 1992; Nittler et al. 1996; Hoppe et al. 2000). Type A and B grains can be distinguished from mainstream grains on the basis of lower $^{12}C/^{13}C$ ratios (for type A ~2–3.5 and for type B ~3.5–10, Hoppe and Ott 1997). Subtypes of carbon stars and novae are suggested sources of these SiC grains. Type Y and Z grains lie to the ^{30}Si-rich side of the slope 1.34 mainstream line in a 3-isotope Si plot. These grains are believed to have formed in carbon stars with lower than solar metallicities.

While the characteristics of the subtypes of presolar SiC grains outlined above is based on isotopic structures of lighter elements, heavy elements such as Sr, Mo, Zr, Nd, Sm, and Ba in SiC grains may also serve as astrophysical diagnostic tools, which can be used to unravel neutron capture nucleosynthesis and mixing processes taking place in the interior of the parent stars. For this reason we performed Ba isotopic measurements of presolar SiC grains, including both mainstream and type X SiC grains.

Barium has seven stable isotopes: ^{130}Ba and ^{132}Ba are pure *p*-process products that are destroyed by *s*-processing, while ^{134}Ba and ^{136}Ba are mainly *s*-process products (~98% and ~100% of their solar abundance as estimated by Arlandini et al. 1999), probably with a small uncertain contribution from the p process. The isotopes 135, 137, and 138 have contributions from both the *r*- and *s*-processes (78%, 42%, and 16%, respectively, of their solar inventory from the *r*-process). As ^{138}Ba is the most abundant isotope, ~80% of the element Ba in the solar system can be considered as having an *s*-process origin (Travaglio et al. 1999).

Barium isotopic anomalies were first discovered in FUN inclusions from the Allende CV3 meteorite by TIMS measurements (McCulloch and Wasserburg 1978). The first Ba measurements of presolar grains were performed by Ott and Begemann (1990) on bulk samples of SiC separated from the Murchison CM2 meteorite. Based on a measured nonsolar $^{134}Ba/^{136}Ba$ ratio, these authors suggested that s-Ba (pure s-process Ba) in SiC grains may be different from the s-Ba inferred for the solar system. The mean neutron exposure that they calculated from the extrapolated $^{138}Ba/^{136}Ba$ for the pure *s*-process component is about a factor of two lower than that inferred for the *s*-process component in the solar system abundance distribution. Furthermore, from a comparison between the abundances of s-Ba and s-Xe Ott and Begemann (1990) concluded that the *s*-process elements may have been implanted into SiC. This initial work was followed by SIMS measurements on bulk SiC samples with different grain sizes from the Murchison meteorite by Zinner et al. (1991). In contrast to Ott and Begemann (1990), these authors argued for condensation of Ba during SiC formation because Ba can be considered a refractory element. The Zinner et al. (1991) results also indicated a decrease of the $^{138}Ba/^{136}Ba$ ratio with grain size, which was interpreted to reflect different neutron exposures. A similar observation was made by Prombo et al. (1993), who studied bulk SiC samples from the Murchison KJ series (KJC ~0.67 μm, KJD ~0.81 μm, KJE ~1.14 μm; Amari et al. 1994) by TIMS. The first measurements of Ba in single SiC grains from the Murchison meteorite were made by Savina et al. (2003), who applied RIMS to the study of grains in the size range 2–5 μm from the Murchison separate KJG (Amari et al. 1994). The isotopes 130 and 132 were not included in the measurements because of their low abundance, and also ^{134}Ba was excluded due to a strong isobaric interference from ^{133}CsH.

Previous Ba isotopic analyses of presolar SiC focused on bulk samples and single grains of the mainstream type from the Murchison meteorite. Only six X grains were studied for their Ba isotopic composition by RIMS (Pellin et al. 2000, 2006). Although some of the data have large errors, enrichments of the heavier isotopes ^{137}Ba and ^{138}Ba are indicated by this work. Beyond SiC from Murchison, only presolar SiC from the Indarch meteorite has been analyzed for its Ba isotopic composition by TIMS for bulk samples and RIMS for single grains (Jennings et al. 2002). Bulk measurements of various grain size fractions showed, especially for the most fine-grained one (0.10–0.15 μm), results similar to those obtained for Murchison by Prombo et al. (1993). The Ba isotopic compositions of 7 single mainstream SiCs were indistinguishable from those of Murchison grains. One of the studied Indarch SiC grains was

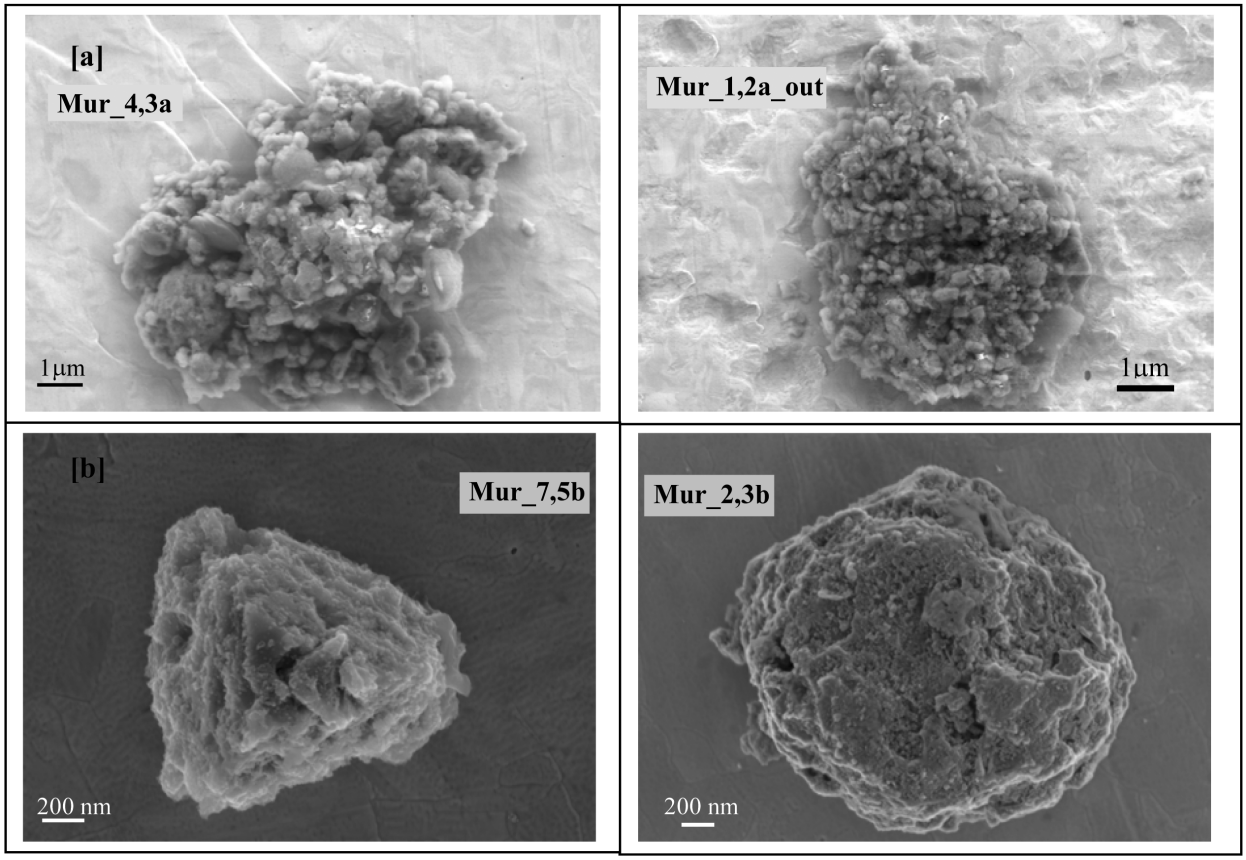

Fig. 1. SEM images of (a) agglomerate-like grains and (b) single mainstream SiCs measured in the present study. Note that the agglomerate-like grains may consist of very fine submicron-size SiC grains; but see also discussion in the text.

a type B grain, which showed near normal (solar) values, i.e., no anomalies. Two presolar silicon nitride grains were also analyzed, but did not contain enough Ba for an isotopic analysis.

In the present paper, we report the results of Ba isotopic measurements on 55 single SiC grains, most of which are of the mainstream type with sizes between 1.0 and 2.6 μm, and on 19 SiC X grains with sizes between 0.2 and 2.3 μm, from the CM2 meteorites Murchison and Murray. In addition, we studied 7 SiC particles from the Murchison meteorite having agglomerate-like morphologies. These samples had sizes ranging from 1.2 to 5.3 μm and may consist of a large number of submicron-size SiC grains or constitute a morphologically and isotopically separate grain population (Fig. 1). Grains with similar morphologies were observed by Heck et al. (2007). A high-resolution NanoSIMS C isotope measurement performed by these authors suggested that these particles are single grains and not agglomerates. In any case, we will refer to these grains here as "agglomerate-like" and will treat their isotope data separately. The measurements were done with the MPI (Mainz) Cameca NanoSIMS 50 ion microprobe (Hillion et al. 1994). The goals of this work are twofold, namely, to obtain a better understanding of the s-process component from low-mass AGB stars contained in SiC grains in the size range considered here and to characterize the Ba isotopic compositions of SiC X grains to gain insight into processes responsible for Ba nucleosynthesis in supernovae.

EXPERIMENTAL

Sample Preparation

The SiC samples were extracted from the Murchison and Murrray (CM) meteorites using the standard method of Amari et al. (1994). The SiC grains were dispersed on clean Au foils using an isopropanol-water-HCl solution. Four mounts with Murchison SiC were prepared and one with Murray SiC, each containing thousands of grains. A field emission scanning electron microscope (Leo 1530) was used to screen the Au mounts in order to determine the particle density (typically on the order of 10–20 SiC grains per 100 μm^2) and grain sizes. The average size of the Murchison SiC grains was measured to be ~1 μm, that of the Murray SiC grains ~0.6 μm. Smaller sizes of typical SiC grains as compared to Murchison SiC have also been reported for the meteorites Indarch (Russell et al. 1997; Gao et al. 1995) and Acfer 094 (Gao et al. 1996), and were inferred for others such as Orgueil (Russell et al. 1997). A possible reason for this size difference is less

destruction/loss of SiC during processing within the solar system (Russell et al. 1997). The extraction process from the meteorite appears unlikely as an explanation, since the chemical separation was done in the same way for both meteorites. Also, parent body processes are unlikely to be responsible for the different sizes, since both meteorites belong to same petrologic type, CM2. Not only are the average sizes different for SiC from the two meteorites, but also the textures of the SiC grains. Murchison grains are more compact and show more pronounced crystal features than Murray SiC grains, which appear to be more porous and to be composed of smaller grains. As noted above, the chemical separation procedure was the same, so the differences in grain size and appearance are somewhat puzzling. However, as the noble gas characteristics of single SiC grains from Murchison and Murray (Heck et al. 2007) are similar, we do not expect that size and surface appearance will have seriously biased our Ba isotope data.

Ion Imaging: Search for X Grains

To identify the rare X grains, one of the Au mounts with SiC grains from Murchison was screened by low mass resolution ion imaging in the MPI (Mainz) IMS3f ion microprobe (Hoppe et al. 2000). Negative secondary ion images of ^{12}C, ^{28}Si, and ^{30}Si were acquired in ~70 areas, each 100 × 100 μm^2 in size (i.e., total area of 0.7 mm^2) using a defocused 10 keV Cs^+ primary ion beam of 5–10 nA with integration times of 1, 1, and 30 s, respectively. Grains with $^{30}Si/^{28}Si$ < 0.8 times the solar value were considered as X grains. Four X grains from Murchison were identified by this technique. Another six Murchison X grains were found by ion imaging using O^- as primary ion and acquisition of positive secondary ion images of ^{24}Mg, ^{28}Si, and ^{30}Si in 5 mm^2 total area with integration times of 2, 2, and 60 s, respectively. Using O^- has the advantage of minimizing problems with $^{133}CsH_x$ interferences during the later Ba measurements (see NanoSIMS Measurements, Barium section). It requires, however, a higher primary current (~20 nA) and longer integration times to obtain sufficiently high positive secondary ion signals, which consumed a large fraction of the small SiC grains. Another two mounts (one each from Murchison and Murray) were screened in the NanoSIMS using O^- primary ions (20–30 pA); positive secondary ion images, 30–40 × 30–40 μm^2 in size, of ^{24}Mg, ^{27}Al, ^{28}Si, ^{29}Si, and ^{30}Si were acquired in multi-collection. This led to the identification of another 9 X grains (4 from Murchison, 5 from Murray). In addition, one Z grain and a grain with high $^{29,30}Si$ enrichments were found using this technique. Advantages of NanoSIMS over IMS3f ion imaging are a) much lower primary current on the sample, thus minimizing material consumption, b) determination of precise Si isotopic ratios during ion imaging itself, c) easy relocation of rare grain types (e.g., X grains) on the mount, and d) the possibility of identifying other rare grain types like the Z grains. The abundance of X grains in Murchison is ~1%. For the Murray sample, only ~0.15% of the SiC grains are X grains. Lower X grain abundances than in Murchison have also been observed for SiC from the meteorites Sahara 97166 (0.4%, Besmehn et al. 2001), Qingzhen (0.1%, Lin et al. 2002), Tieschitz (0.3%, Nittler 1996), and Indarch (<0.1%, Besmehn and Hoppe 2001). However, the abundance estimates should be taken with great care as, e.g., the X grain abundance reported by Nittler (1996) for Tieschitz is only a lower limit because of contamination with terrestrial SiC. For Indarch, Nittler (1996) found an X grain abundance of 0.9%, clearly higher than the value reported by Besmehn and Hoppe (2001) and consistent with the Murchison abundance estimates.

Grain Selection

The 19 X grains identified by ion imaging (5 from Murray and 14 from Murchison) were subsequently relocated in the SEM. Their sizes were measured to be between 0.2 and 2.3 μm. In addition, from the grain mount not screened by ion imaging, 44 single SiC grains (1.0–2.6 μm) and 7 agglomerate-like grains (1.2–5.3 μm) were preselected in the SEM (Leo 1530 FESEM) for the study of Ba isotopic compositions in the NanoSIMS (Fig. 1). Main selection criterion was a grain size >1 μm. An additional 11 grains were randomly selected in the NanoSIMS. In these cases, no SEM and grain size information is available.

NanoSIMS Measurements

Carbon and Silicon

Carbon and Si isotopic measurements for mainstream grains were done following the Ba measurements when sufficient grain material was left. A Cs^+ primary ion beam (~100 nm, <1 pA) was rastered (256 × 256 pixels) over the grains. Raster sizes were 1 × 1 to 6 × 6 μm^2, depending on the size of the analyzed grains. Fourteen out of the 55 single grains could be analyzed for Si and 9 for C. Also, most of the X grains found by ion imaging in the IMS3f were remeasured for their Si isotopic composition in the NanoSIMS prior to Ba analysis (except for seven very small ones). All were confirmed to be X grains (large depletions in ^{29}Si and ^{30}Si). Since these measurements preceded the Ba measurement, we used O^- as primary ion in order to minimize the CsH_x interference problem during Ba measurements. We also kept measurement times as short as possible. The O^- beam was defocused (~2 μm) for some of the Murchison grains in the initial stage of our study. It was rastered (raster size ~2× grain size, beam diameter ~300 nm) in the case of the other Murchison and Murray grains. Synthetic SiC (for Si) and synthetic SiC doped with N (for C measurements) were used as isotope standards. Standard measurements were done at the

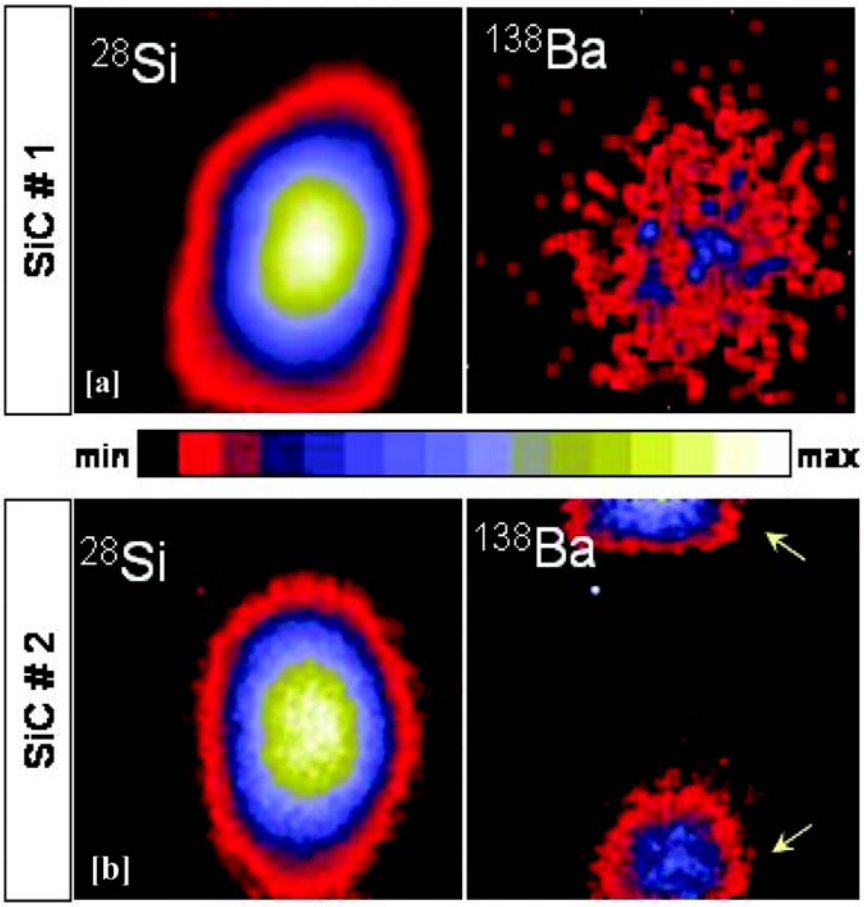

Fig. 2. ^{28}Si and ^{138}Ba ion images (4 × 4 μm^2) of two mainstream silicon carbide grains. The ^{138}Ba ion image of the grain SiC#1 (a) indicates that Ba is intrinsic to the grain itself (coincides with the Si ion image), whereas for grain SiC#2 (b), the ^{138}Ba ions originate clearly from the surroundings (indicated by arrows), i.e., this Ba is contamination.

beginning and at the end of each measurement session. Reproducibility of Si isotopic ratios on synthetic SiC was ~4‰ ($^{29}Si/^{28}Si$) and ~6‰ ($^{30}Si/^{28}Si$) for O^- primary ions and, respectively, ~3‰ for both Si isotopic ratios for Cs^+ primary ions. For the C isotope ratio measurements, the reproducibility was better than 4‰.

Silicon and Barium Ion Imaging

High-resolution NanoSIMS ion images of $^{28}Si^+$ and $^{138}Ba^+$ were acquired in order to ensure that Ba was intrinsic to the SiC grains of interest. A focused O^- ion beam of several pA was focused into a spot of ~300 nm and rastered over the grains. Raster sizes were between 1 × 1 and 6 × 6 μm^2. Silicon-barium imaging turned out to be an important tool to identify grains contaminated by Ba from the surroundings. An example of such a Ba-contaminated grain can be seen in Fig. 2, where ion images of ^{28}Si and ^{138}Ba for two different SiC grains are shown. Figure 2a shows a typical grain (analyzed further for Ba isotopic composition) for which all Ba secondary ions are intrinsic to the grain. The ^{138}Ba ion image displayed in Fig. 2b, however, indicates high Ba concentrations in the surroundings of the grain of interest. This could be due to Ba-rich phases (e.g., hibonite) (Amari et al. 1994) or it could be intrinsic to the gold substrate as also observed by Amari et al. (1995). Such grains were excluded from Ba isotopic analyses.

Barium

Ba isotopic ratios were measured on the 19 X grains, the additional 55 single grains, and the 7 SiC agglomerate-like grains. Three of the X grains and 32 of the additional grains were large enough and/or had high enough Ba content to obtain useful results. For Ba measurements, the NanoSIMS was operated in a combined multi-collection and peak-jumping mode, using four different magnetic field settings and four different electron multiplier detectors. The primary beam of O^- (~10 pA) was defocused (~2 μm) for some of the Murchison grains and rastered (raster size ~2× grain size, beam diameter ~300 nm) for most of the Murchison and all Murray grains. The following isotopes were included in the measurement: ^{134}Ba, ^{135}Ba, ^{136}Ba, ^{137}Ba, ^{138}Ba, and ^{28}Si, ^{88}Sr, ^{90}Zr, ^{133}Cs, ^{139}La, and ^{140}Ce. The isotopes ^{130}Ba and ^{132}Ba were not included in the measurements because of their low isotopic abundances (~0.1% in normal Ba). Synthetic SiC,

NIST SRM611 glass, and barium nitrate (BaN_2O_6) were used as isotope standards. Relative sensitivity factors (RSF) for Ba and the other trace elements Sr, Zr, Cs, La, and Ce were measured on the NIST SRM611 standard. Normalized to Si we obtained RSF values of 12.1 (Ba), 11.1 (Sr), 2.1 (Zr), 31 (Cs), 4.0 (La), and 3.9 (Ce), respectively. These values were used to calculate trace element abundances in the presolar SiC grains (see Table 1). The reproducibility of Ba isotopic measurements on the standards within a given measurement session was on average 1.8% ($^{134}Ba/^{136}Ba$), 1.1% ($^{135}Ba/^{136}Ba$), 1.6% ($^{137}Ba/^{136}Ba$), and 3.3% ($^{138}Ba/^{136}Ba$), respectively. The reproducibility is not included in the errors given in Table 2, but can be considered negligible in view of the larger errors from counting statistics and CsH_x interference correction (see below).

As it turned out, grains that had been bombarded with Cs prior to the Ba analyses sometimes showed large apparent excesses in ^{134}Ba. Since these are larger for grains with high Cs concentrations, this can be attributed to the presence of a CsH interference, which, at mass resolution ~2500–3000, was not separated from ^{134}Ba.

There are three possible sources of Cs, namely, intrinsic (i.e., stellar) Cs, surface contamination on the SiC grains and the Au mounts, and implanted Cs from ion imaging. For 26 out of the 32 grains where Ba isotope results were obtained, the Cs correction was either negligible or we feel confident about the correction scheme applied as explained below. Measured $^{134}Ba/^{136}Ba$ ratios for these are plotted as a function of Cs/Ba ratio in Fig. 3. As apparent, for grains with low Cs/Ba the effect of the interference is negligible and the ratios on average agree with the $^{134}Ba/^{136}Ba$ ratio measured on bulk Murchison SiC samples by Prombo et al. (1993). For higher Cs/Ba, the measured ratios R_{mea} scatter around a relationship

$$R_{mea} = R_0 + a * (\log([Cs/Ba] + 2.5) \quad (1)$$

where $R = {}^{134}Ba/^{136}Ba$, $R_0 = 0.325 \pm 0.013$, and $a = 0.0807 \pm 0.0067$ are the parameters from the weighted linear regression in Fig. 3. The constant 2.5 in the equation was chosen so that R_0 matches the average ratio measured at low Cs/Ba, i.e., the Prombo et al. bulk value. The CsH-corrected $^{134}Ba/^{136}Ba$ ratio of individual grains was then calculated from

$$R_{true} = R_{mea}/f \quad (2)$$

where

$$f = 1 + a/R_0 * (\log[Cs/Ba] + 2.5) \quad (3)$$

Note that obviously the true ratios are independent of Cs/Ba and the correction relies on the average trend of $^{134}Ba/^{136}Ba$ with Cs/Ba around which the measured ratios scatter. Hence the correction accounts for the interference, while at the same time keeping the individuality of each data point.

Uncertainties from the correction are included in the given errors (1σ). As apparently CsH_x interferences were present also on the other Ba isotopes, a similar correction scheme, based on a logarithmic dependence and keeping the constant 2.5 (defining the cutoff below which no correction was necessary for $^{134}Ba/^{136}Ba$), was applied to the other Ba isotopic ratios as well. We note that the isotopic ratios of grains that were significantly corrected for CsH_x do not differ systematically from those grains that were not contaminated by large amounts of Cs.

RESULTS

The Ba isotopic compositions along with Si and C compositions for 26 (likely) mainstream grains, 3 X grains, and the agglomerate-like grains are given in Table 2. Barium isotopic ratios (relative to ^{136}Ba) are given as delta values, i.e., in permil deviation from the solar ratios. Errors (1σ) are based on counting statistics and the errors from the CsH_x correction. For the remaining 29 mainstream and 16 X grains that were measured for Ba, no data are given in Table 2 because of either too low Ba secondary ion intensities or because the Cs interference correction was deemed too uncertain. Among the grains not listed is a Z grain ($\delta^{29}Si = -68 \pm 22‰$, $\delta^{30}Si = 178 \pm 28‰$) and a grain with large enrichments in both ^{29}Si and ^{30}Si ($\delta^{29}Si = 490 \pm 22‰$, $\delta^{30}Si = 553 \pm 28‰$).

Single Mainstream Grains and Agglomerate-Like Grains

Except for one X grain, all individual SiC grains for which both C and Si isotopic ratios were measured (9 grains) belong to the mainstream group, as evidenced from their C and Si isotopic signature. These grains have $^{12}C/^{13}C$ ratios ranging from 20 to 83, except for one grain with $^{12}C/^{13}C = 10.8 \pm 0.2$, which is close to the signature of A/B-type grains. Si isotopic compositions (measured in 14 mainstream grains) range from −35 to +143‰ for $\delta^{29}Si$ and from −2 to +125‰ for $\delta^{30}Si$. Within errors all grains lie along the characteristic line with slope 1.34 for mainstream (and type A/B) grains. As the mainstream grains make up ~90% of presolar SiC (Hoppe and Ott 1997), we will assume that all of the grains for which no C and/or Si data are available are of the mainstream type. For six of the agglomerate-like grains the Si isotopic composition was measured, and in five cases it plots on or very close to the mainstream line. However, in one case (1,4b_out; Table 2) Si isotopic ratios are slightly shifted to the ^{30}Si-rich side of the mainstream line.

The ^{136}Ba-normalized Ba isotopic patterns for both single and agglomerate-like grains follow the same trend, with enrichments in ^{134}Ba (most grains), and depletions in ^{135}Ba, ^{137}Ba, and ^{138}Ba (Fig. 4). Weighted average values (Table 3) are also indicated. Compared to the previous measurements on single SiC grains (Savina et al. 2003), the range in Ba isotopic compositions is more restricted and also more extreme. The patterns are qualitatively consistent with those from previous studies (Ott and Begemann 1990; Zinner et al. 1991; Prombo et al. 1993; Savina et al. 2003; Barzyk

Table 1. Trace element concentrations, normalized to Si and CI, for presolar SiC grains of this study. For comparison, the Amari et al. (1995) data for fine-grained SiC from Murchison separates KJA-KJF are given. Uncertainty in abundance calculation is ~6–10%.

Size (μm)	Sample	$[Sr]_{Si-CI}$	$[Zr]_{Si-CI}$	$[Cs]_{Si-CI}$	$[La]_{Si-CI}$	$[Ce]_{Si-CI}$	$[Ba]_{Si-CI}$
Agglomerate-like grains							
2.2	1,4b_out	0.3	8.3	0.3	13.4	10.0	4.6
5.3	1,2a_out	0.3	6.2	0.1	6.4	5.4	3.9
3.0	2,2b	0.3	3.8	0.1	3.5	3.4	1.6
1.2	2,6a	0.4	5.3	0.2	8.8	8.8	6.0
5.3	4,3a	0.3	16.1	0.3	8.1	6.5	3.2
3.7	3,1a_out	0.4	6.0	0.3	9.0	7.7	4.1
3.3	3,1b_out	0.6	6.5	1.4	19.2	13.1	6.9
Mainstream grains (single)							
1.7	8,2a	0.2	1.8	0.6	8.5	7.8	2.4
1.5	7,5b	0.2	5.8	0.7	11.2	8.2	6.2
2.4	7,5a	0.1	1.6	0.2	3.2	2.8	1.9
2.6	6,8a_out	1.1	2.2	0.3	3.9	3.7	3.3
2.1	2,3b	0.3	0.8	0.8	13.6	11.7	1.3
1.6	3,8a_out	0.1	2.6	3.6	19.4	11.4	12.7
1.2	8,3a_out	0.1	22.5	111.2	12.6	7.3	6.0
1.3	5,6c	0.2	5.9	6103	13.3	4.8	8.9
1.2	5,7a	0.1	31.2	426.2	46.5	37.3	16.4
1.3	6,1b	0.3	31.6	2233	54.6	26.5	18.3
1.2	6,6c	1.1	40.2	57,555	37.0	31.5	3.0
1.0	4,7b_out	1.4	8.9	59.9	77.1	63.8	28.6
1.2	4,8b	2.7	3.9	5.5	28.5	27.6	36.8
1.8	4,4a_out	0.3	5.2	24.7	16.7	12.4	2.5
–	4,4a_out_a	0.1	1.8	2.0	8.3	6.8	0.5
1.6	8,4a_out	1.6	17.9	379.9	30.4	21.7	16.2
–	629#1	0.5	5.4	[a]	20.6	31.8	6.2
–	696#1	0.1	2.1	[a]	35.0	31.3	1.2
–	kkm3_5	5.4	5.4	16.2	146.7	107.7	132.7
–	kkm3_12	0.8	8.4	13.4	42.4	17.9	10.1
–	kkm3_15	0.8	20.3	16.9	40.4	15.1	21.4
–	kkm3_16	2.3	10.8	15.2	15.2	12.6	17.2
–	kkm3_23	0.8	6.9	23.0	17.4	11.9	8.7
–	kkm3_33	4.2	13.3	59.0	1154	52.4	25.0
–	kkm3_37	1.7	6.0	16.9	148.6	52.5	60.4
–	kkm3_39	0.5	1.4	16.0	45.2	28.0	12.9
X grains							
2.3	629#2	0.5	3.4	[a]	37.1	23.1	4.9
1.3	373#3	1.1	3.0	[a]	22.0	30.4	3.9
–	311#10	1.2	2.9	10.0	32.5	7.5	12.4
–	930#3	9.1	21.2	58.4	628.4	251.0	57.1
–	979#9	2.7	0.0	150.6	50.6	21.5	18.1
–	115#12	1.4	5.6	38.5	46.6	20.5	27.1
–	211#9	0.3	0.5	4.0	12.3	3.6	2.4
–	934#2	1.8	37.1	932.1	214.4	80.8	102.0
–	murC3@4_8#49	1.0	0.9	47.8	29.3	2.7	4.5
–	murC3@1_5#36	0.9	0.7	490.1	9.8	5.2	6.9
–	murC3@1_5#44	1.6	2.0	239.1	55.4	8.1	25.8
–	murC3@1_42#51	0.6	1.0	51.4	6.7	2.0	5.1
–	murC3@2_43#35	7.7	33.4	744.0	665.4	47.3	30.4
–	murC3@2_58#28	2.6	6.7	26.6	16.5	3.9	5.8
–	SiC 8-13#23[b]	0.3	4.2	70.2	81.1	36.6	9.5
–	SiC 4_27[b]	0.6	1.6	47.6	6.1	3.8	3.5
–	SiC 3_2#3[b]	0.1	0.7	6.5	5.9	1.9	5.1

Table 1. *Continued.* Trace element concentrations, normalized to Si and CI, for presolar SiC grains of this study. For comparison, the Amari et al. (1995) data for fine-grained SiC from Murchison separates KJA-KJF are given. Uncertainty in abundance calculation is ~6–10%.

Size (μm)	Sample	$[Sr]_{Si\text{-}CI}$	$[Zr]_{Si\text{-}CI}$	$[Cs]_{Si\text{-}CI}$	$[La]_{Si\text{-}CI}$	$[Ce]_{Si\text{-}CI}$	$[Ba]_{Si\text{-}CI}$
Amari et al. 1995							
0.38	KJA	1.8	43.6			10.1	27.35
0.49	KJB	1.18	27.9			18.7	15.6
0.67	KJC	1.07	19.6			12.9	10.8
0.81	KJD	1.3	46.2			13.5	10.36
1.14	KJE	1.3	63.4			12.9	11.58
1.86	KJF	0.86	478.1			10.3	8.17

[a]Heavy Cs contamination due to use of Cs-beam in the search for X grains.
[b]X grains from the Murray meteorite. Two more grains from Murray are not listed because no counts were detected for the trace elements.

Table 2. Ba isotopic compositions, given as deviation in permil from the solar $^{x}Ba/^{136}Ba$ ratios, and C and Si isotopic data for SiC agglomerate-like grains and single grains. Errors are 1σ.

Sample	$\delta^{134}Ba$ (‰)	$\delta^{135}Ba$ (‰)	$\delta^{137}Ba$ (‰)	$\delta^{138}Ba$ (‰)	$\delta^{29}Si$ (‰)	$\delta^{30}Si$ (‰)	$^{12}C/^{13}C$
Agglomerate-like grains							
1,4b_out	94 ± 130	–665 ± 43	–437 ± 52	–311 ± 45	–47 ± 8	41 ± 12.6	
1,2a_out	220 ± 109	–733 ± 29	–394 ± 41	–301 ± 35	–24 ± 8	21 ± 12.8	
2,2b	372 ± 91	–568 ± 31	–404 ± 32	–356 ± 26	52 ± 12	56 ± 20.6	
2,6a	193 ± 157	–659 ± 49	–550 ± 49	–385 ± 46			
4,3a	208 ± 131	–627 ± 45	–477 ± 47	–423 ± 37	2 ± 9	2 ± 16.1	
3,1a_out	100 ± 74	–677 ± 24	–475 ± 28	–338 ± 25	41 ± 6	51 ± 10.2	
3,1b_out	–57 ± 63	–633 ± 25	–558 ± 24	–522 ± 18	–7 ± 8	36 ± 12.9	
Mainstream grains (single)							
8,2a	222 ± 273	–665 ± 85	–437 ± 104	–378 ± 84	17 ± 10	–2 ± 12	73.3 ± 1.1
7,5b	125 ± 200	–546 ± 79	–229 ± 99	–345 ± 66	38 ± 12	54 ± 15	44.1 ± 1.0
7,5a	99 ± 101	–642 ± 35	–424 ± 41	–431 ± 29	127 ± 3	112 ± 4	51.4 ± 0.4
6,8a_out	182 ± 58	–521 ± 23	–357 ± 24	–345 ± 18	42 ± 8	31 ± 10	60.1 ± 1.6
2,3b	141 ± 193	–355 ± 104	–279 ± 96	–366 ± 66	143 ± 3	125 ± 6	22.0 ± 0.4
3,8a_out	–61 ± 128	–765 ± 40	–314 ± 68	–212 ± 58	–20 ± 4	10 ± 5	
8,3a_out	26 ± 103	–679 ± 38	–269 ± 58	–199 ± 47			
5,6c	175 ± 122	–461 ± 64	–88 ± 79	–103 ± 60	17 ± 10	21 ± 10	
5,7a	–34 ± 75	–622 ± 32	–308 ± 40	–218 ± 33			
6,1b	–84 ± 116	–388 ± 77	–79 ± 89	–92 ± 69	83 ± 3	84 ± 3	
6,6c	158 ± 169	–499 ± 85	–384 ± 92	–516 ± 52	–14 ± 2	14 ± 2	
4,7b_out	–17 ± 124	–742 ± 41	–245 ± 72	8 ± 72	–6 ± 13	21 ± 17	
4,8b	47 ± 95	–630 ± 35	–312 ± 46	–168 ± 41			
4,4a_out	113 ± 176	–696 ± 60	–63 ± 118	16 ± 98			
4,4a_out_a	368 ± 232	–656 ± 74	–302 ±104	–201 ± 88			
8,4a_out	154 ± 205	–529 ± 93	–316 ± 108	–330 ± 77			
629#1	88 ± 93	–589 ± 45	–301 ± 50	237 ± 61			
696#1	352 ± 137	–702 ± 43	–387 ± 63	–353 ± 46			
Kkm3_5	493 ± 262	–711 ± 62	–233 ± 106	–146 ± 92	75 ± 14	54 ± 16	83.2 ± 0.6
Kkm3_12	106 ±108	–445 ± 52	–352 ± 52	–337 ± 39			
Kkm3_15	324 ± 238	–345 ± 112	46 ± 140	–300 ± 79	45 ± 25	25 ± 30	10.8 ± 0.2
Kkm3_16	65 ± 332	–592 ± 137	–233 ± 182	–261 ± 134	–35 ± 17	16 ± 21	20.3 ± 0.3
Kkm3_23	210 ± 339	–353 ± 170	–218 ± 176	–141 ± 150			
Kkm3_33	206 ± 158	–483 ± 70	–210 ± 84	–359 ± 54	–3 ± 26	19 ± 32	78.2 ± 3.6
Kkm3_37	–39 ± 68	–701 ± 24	–321 ± 35	–164 ± 32			
Kkm3_39	–134 ± 131	–630 ± 62	–414 ± 71	–253 ± 65			
Type X							
629#2	261 ± 137	–371 ± 81	243 ± 111	1329 ± 160	–271 ± 8	–475 ± 8	
373#3	132 ± 214	–329 ± 152	166 ± 205	812 ± 256	–289 ± 3	–508 ± 4	286 ± 5
311#10	407 ± 180	–373 ± 82	–177 ± 87	321 ± 107		–525[a]	

[a]Data from ion imaging (IMS3f).

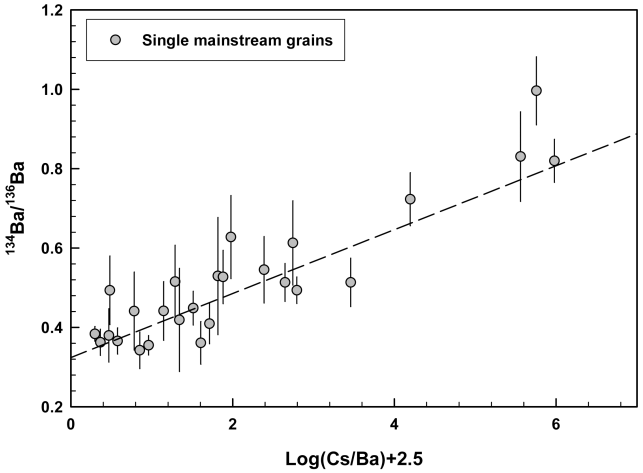

Fig. 3. Measured $^{134}Ba/^{136}Ba$ ratio versus the Cs/Ba ratio. The positive correlation is suggestive of a contribution from ^{133}CsH to ^{134}Ba. A correction was made to the measured ^{134}Ba on the basis of a weighted linear regression (line) which has an intercept at 0.325 and slope of 0.0807 (see discussion in the text). Errors are 1σ.

et al. 2006, 2007). On average, $^{134}Ba/^{136}Ba$ and $^{135}Ba/^{136}Ba$ in the agglomerate-like grains ($\delta^{134}Ba = 117 \pm 59$, $\delta^{135}Ba = -654 \pm 20$; 1σ errors) are consistent with those of single grains ($\delta^{134}Ba = 77 \pm 24$, $\delta^{135}Ba = -621 \pm 19$). Average $^{137}Ba/^{136}Ba$ and $^{138}Ba/^{136}Ba$, on the other hand, are lower in the agglomerate-like grains ($\delta^{137}Ba = -483 \pm 26$, $\delta^{138}Ba = -412 \pm 36$ versus $\delta^{137}Ba = -319 \pm 16$, $\delta^{138}Ba = -277 \pm 27$; 1σ errors). Barium concentrations (Table 1) range from 25 to 107 ppm (1.6–6.9 × the Si-normalized CI concentration) in agglomerate-like grains and from 8 to 2047 ppm in single grains (0.5–133 × the Si-normalized CI concentration).

In Figs. 5a–c, we display our Ba data for single mainstream (verified and assumed) grains and the agglomerate-like grains in three isotope plots. For comparison we have also included the Ba data obtained for SiC bulk samples by Ott and Begemann (1990), Zinner et al. (1991), and Prombo et al. (1993) and for single SiC grains with sizes 2–5 μm by Savina et al. (2003). ^{134}Ba was not reported by Savina and co-workers. In Fig. 5a, data points with errors larger than 150‰ for $\delta^{134}Ba$ are excluded. Similarly, in Figs. 5b and 5c grains with errors of more than 100‰ in $\delta^{135}Ba$, $\delta^{137}Ba$, and/or $\delta^{138}Ba$ (both from this work and Savina et al. 2003) are not shown. The solid line in all δ-plots is the mixing line of Ba with solar composition (N component) and pure *s*-process composition (G component) as calculated by Prombo et al. (1993). ^{134}Ba (Fig. 5a) and ^{138}Ba (Fig. 5c) in single grains scatter around the respective mixing lines, with the scatter in $\delta^{138}Ba$ and $\delta^{134}Ba$ quite large. In contrast, $\delta^{137}Ba$ in single grains tends to plot above the mixing line, while the agglomerate-like grains plot below. At present, we have no good explanation for this. In principle it may be related to problems with the interference correction, but this seems unlikely, since the weighted average of the 15

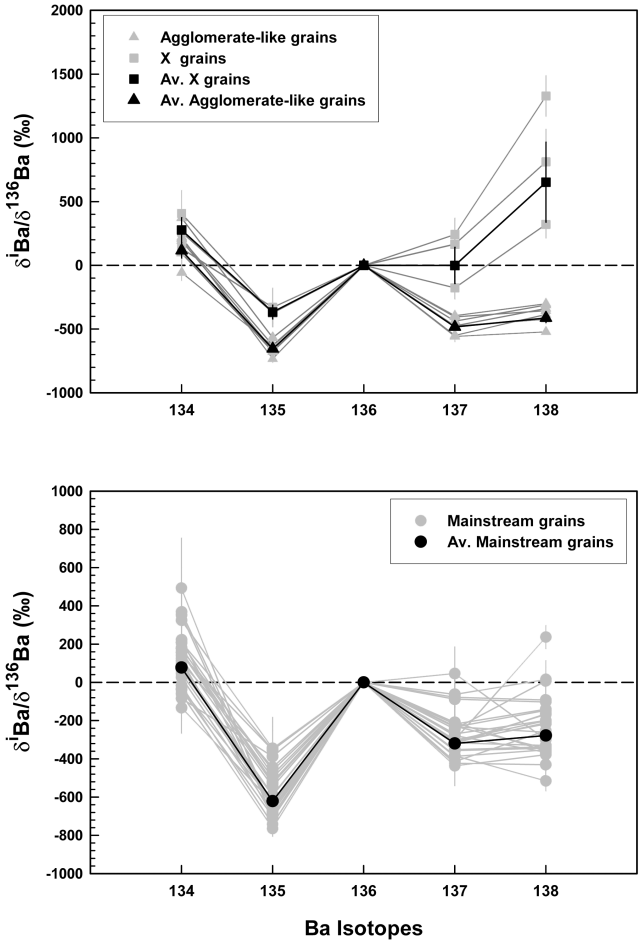

Fig. 4. Ba isotopic compositions of (a) 7 SiC agglomerate-like grains and 3 SiC X grains and (b) 26 individual presolar SiC mainstream grains. Errors are 1σ. The weighted average compositions of the agglomerate-like grains ($\delta^{134}Ba = 117 \pm 59$, $\delta^{135}Ba = -654 \pm 20$, $\delta^{137}Ba = -483 \pm 26$, $\delta^{138}Ba = -412 \pm 36$), X grains ($\delta^{134}Ba = 277 \pm 97$, $\delta^{135}Ba = -366 \pm 54$, $\delta^{137}Ba = -1 \pm 142$, $\delta^{138}Ba = 652 \pm 314$) and for the mainstream grains ($\delta^{134}Ba = 77 \pm 24$, $\delta^{135}Ba = -621 \pm 19$, $\delta^{137}Ba = -319 \pm 16$, $\delta^{138}Ba = -277 \pm 27$) are shown by black symbols.

individual grains with less than 10% correction agrees with that for all 26 grains within 10‰. We cannot completely rule out a problem with instrumental mass fractionation correction (including both true mass fractionation and relative counter efficiencies), which for $^{137}Ba/^{136}Ba$ was significantly larger and variable (from session to session) than for the other ratios. The agglomerate-like grains with their low Cs contents are not affected by the correction at all, however.

Type X Grains

The enrichments in ^{28}Si as seen in 19 Murchison SiC grains characterize them as type X grains. The most extreme grain has $\delta^{29}Si = -502 \pm 29‰$ and $\delta^{30}Si = -553 \pm 28‰$. The C isotopic composition was measured only in one of the grains; we found a high $^{12}C/^{13}C$ ratio of 287.

Table 3. Average Ba isotopic compositions of presolar SiC studied here and from previous studies.

Study	Sample	Fraction	δ^{134}Ba (‰)	δ^{135}Ba (‰)	δ^{137}Ba (‰)	δ^{138}Ba (‰)
Ott and Begemann 1990	Bulk, Murchison	R1CPD	33 ± 2	–255 ± 2	–159 ± 1	–98 ± 1
Zinner et al. 1991	Bulk, Murchison	KJE		–560 ± 51	–358 ± 36	–230 ± 27
Prombo et al. 1993	Bulk, Murchison	KJ	84	–658	–409	–250
s-process (Prombo et al. 1993)	Bulk, Murchison	KJ	108	–839	–521	–319
Jennings et al. 2002	Indarch	6 MS SiCs,	94 ± 74	–756 ± 20	–473 ± 27	–362 ± 24
		1 B grain	–5 ± 179	–49 ± 126	–86 ± 108	–7 ± 93
Savina et al. 2003[a]	Murchison	15 MS SiCs (KJG)		–478 ± 70	–242 ± 44	–206 ± 25
This work	Murchison	7 agglomerate-like grains	117 ± 59	–654 ± 20	–483 ± 26	–412 ± 36
This work	Murchison and Murray	26 mainstream grains	77 ± 24	–621 ± 19	–319 ± 16	–277 ± 27

[a]Weighted average is given; errors are 1σ.

Two of the Murray X grains, about 200 nm in size, showed no Ba at all. For the remaining three Murray X grains, ranging in size from 300 to 600 nm, the typical ^{138}Ba secondary ion signal was only 1 cps, too low to acquire sufficiently precise Ba isotopic data. The same holds for 11 Murchison X grains of unknown size. In spite of the longest possible measurement times it was impossible to collect enough secondary ions to obtain sufficiently precise Ba data. In two Murchison X grains with sizes of 1.3 and 2.3 μm, respectively, the Ba secondary ion intensities were high enough to obtain Ba isotopic data with acceptable precision. The same holds for one Murchison X grain of unknown size. These three X grains exhibit a Ba isotopic pattern, normalized to ^{136}Ba and solar, which is characterized by depletions in ^{135}Ba, enrichments in ^{134}Ba and ^{138}Ba, and close to normal ^{137}Ba (Fig. 4). Relative to the mainstream grains ^{135}Ba/^{136}Ba, ^{137}Ba/^{136}Ba, and ^{138}Ba/^{136}Ba ratios are higher. In the three-isotope plot δ^{137}Ba versus δ^{135}Ba one (out of three) of the X grains falls on the line that connects the N with the G component (Fig. 5b), while in a plot δ^{138}Ba versus δ^{135}Ba all clearly plot off the mixing line (Fig. 5c). The Ba isotopic compositions of bulk samples (dominated by mainstream grains) and averages of the single mainstream grains of this study plot on or close to this line, which underlines the different nature of Ba in X grains compared to that in mainstream grains. Previous data for Ba isotopic compositions of X grains were obtained by Pellin et al. (2000, 2006). In the earlier work (Pellin et al. 2000), these authors found very large excesses in ^{138}Ba in their two grains (+1890‰, +3808‰). In spite of huge errors of 900‰ and 2150‰ (2σ), respectively, a clear excess is indicated in ^{138}Ba. Among the four additional X grains of Pellin et al. (2006), one has ^{138}Ba enhanced similarly to the grains of this study, while the other three have close to normal ^{138}Ba/^{136}Ba.

The Ba concentrations in 19 X grains of this study range from 37 to 1570 ppm (2.4–102 × the Si-normalized CI concentration) (Table 1), except for the two grains with no Ba counts. The average is 263 ppm, which is similar to what is observed in mainstream grains (273 ppm). Although mainstream grains and X grains have similar Ba concentrations, Ba measurements on X grains turned out to be more difficult because of their smaller grain size.

Trace Element Concentrations

Measured trace element (Sr, Zr, Cs, Ba, La, Ce) concentrations (normalized to Si and CI) are listed in Table 1. For comparison, the results obtained for SiC bulk samples of different grain size (Amari et al. 1995) are also given. The concentrations are based on the measurement of the most abundant isotope in each case (^{88}Sr, ^{90}Zr, ^{133}Cs, ^{138}Ba, ^{139}La, and ^{140}Ce). Figure 6 shows the various trace element abundance correlation plots. Important points to note here are:

1. A spread of two orders of magnitude is seen in all of the trace elements measured, except for Cs (not shown in Fig. 6), which shows a spread over 6 orders of magnitude due to implanted Cs from ion imaging. The bulk measurements of the fine-grained samples KJA-KJG (Amari et al. 1995) for Sr and Ce fall within the range defined by the mainstream grains analyzed in this work. Zr data from Amari et al. (1995) are slightly higher than our values.
2. No systematic difference is obvious for the 19 X grains compared to the single mainstream grains and the agglomerate-like grains.
3. Normalized to Si and CI, Sr is less abundant than Ba by an order of magnitude. La and Ce are higher.
4. Except for Cs and Zr, a reasonably good correlation exists between Ba and the other trace elements measured, i.e., Sr, La, and Ce.
5. Zirconium, La, Ba, and Ce are enriched relative to Si and CI, only Sr is depleted in most of the grains.
6. A comparison to the single grain measurements of Amari et al. (1995) on KJH grains (3–10 μm; S. Amari, personal communication) indicates a trend for trace element concentrations to be lower for larger grain sizes.

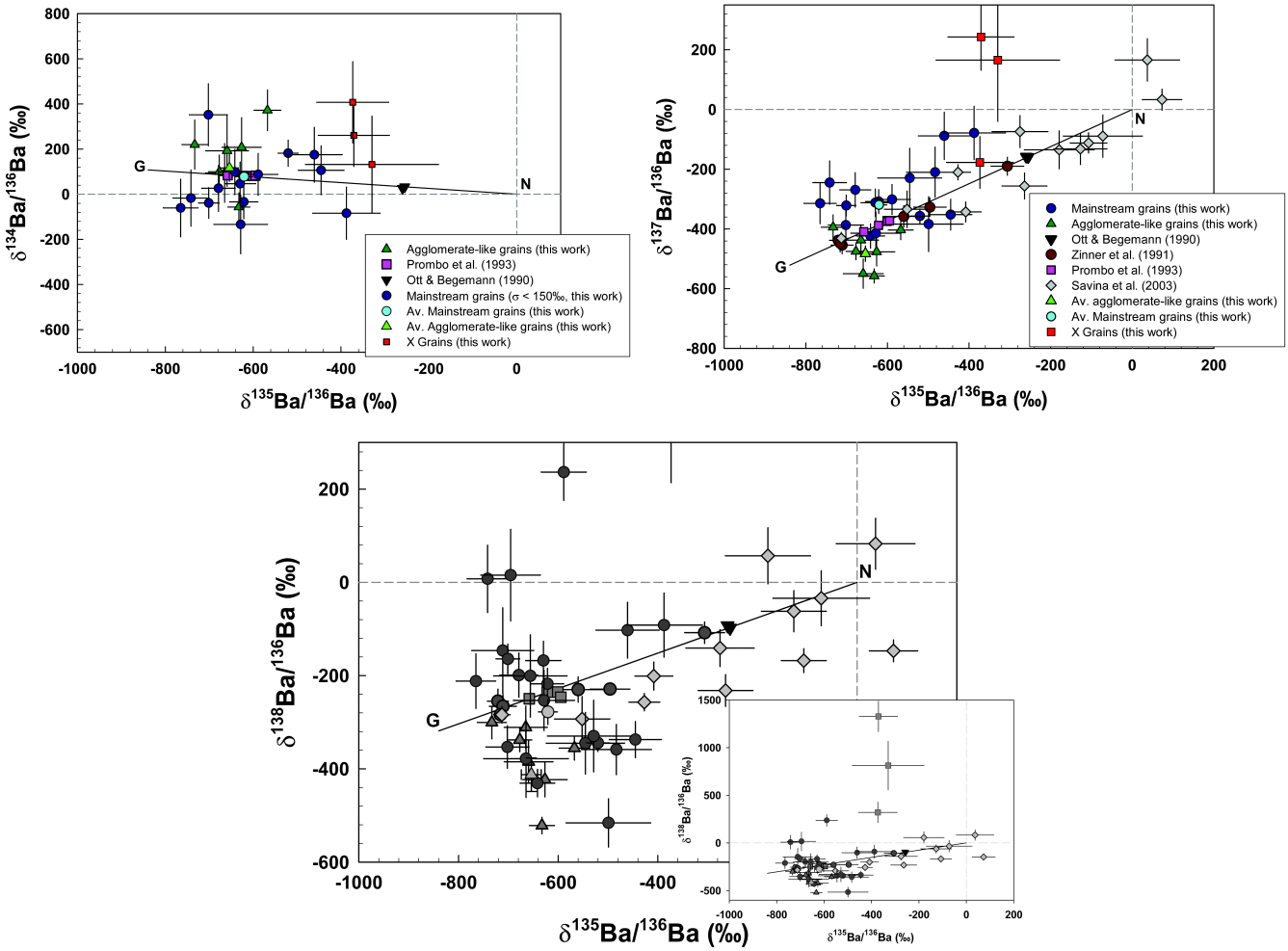

Fig. 5. Barium three-isotope plots for SiC agglomerate-like grains, single mainstream grains, and X grains. a) δ^{134}Ba versus δ^{135}Ba. b) δ^{137}Ba versus δ^{135}Ba. c) δ^{138}Ba versus δ^{135}Ba. Errors are 1σ. Grains with errors larger than 150‰ for δ^{134}Ba and larger than 100‰ in $\delta^{135, 137, 138}$Ba are not plotted. Bulk data from SIMS and TIMS (Ott and Begemann 1990; Zinner et al. 1991; Prombo et al. 1993) are shown for comparison. Single grain data from Savina et al. (2003) plot closer to the normal solar composition than do the grains of this study. The mixing line of the G and N components (Prombo et al. 1993) is also shown.

DISCUSSION

We will discuss the results obtained for agglomerate-like grains and single (likely) mainstream grains together because even if the former are composed of a large number of submicron-size grains, they can be assumed to be dominated by mainstream grains (see the following section). The X grain data and likely nucleosynthetic processes responsible for the production of Ba isotopes in supernova environments are discussed in separate sections (see the X Grains, the r-Process, and Supernovae section, and the Neutron Bursts, Weak s-Process, and Other Alternatives section). In the Source of Ba in SiC: Ion Implantation versus Condensation section, we will finally discuss the question of how Ba and other trace elements were incorporated into presolar SiC grains.

Mainstream Grains and *s*-Process Nucleosynthesis of Ba in AGB Stars

It is now well established that SiC mainstream grains formed in the circumstellar disks surrounding low-mass (1–3 $M_\odot$) AGB stars (e.g., Lugaro et al. 2003). In AGB stars, Ba, like other heavy elements beyond iron, is produced by the s-process operating in the He intershell, the region between the helium-burning and hydrogen-burning shells. There are two main neutron sources, namely the reactions $^{13}C(\alpha,n)^{16}O$ and $^{22}Ne(\alpha,n)^{25}Mg$. The ^{13}C neutron source is dominant in low-mass AGB stars due to the temperature constraints (~10^8 K). Here, temperatures reached in the He intershell lead to only marginal additional activation of the ^{22}Ne neutron source (see below). After a limited number of thermal runaways (TP, i.e., thermal pulses) of the helium shell, the

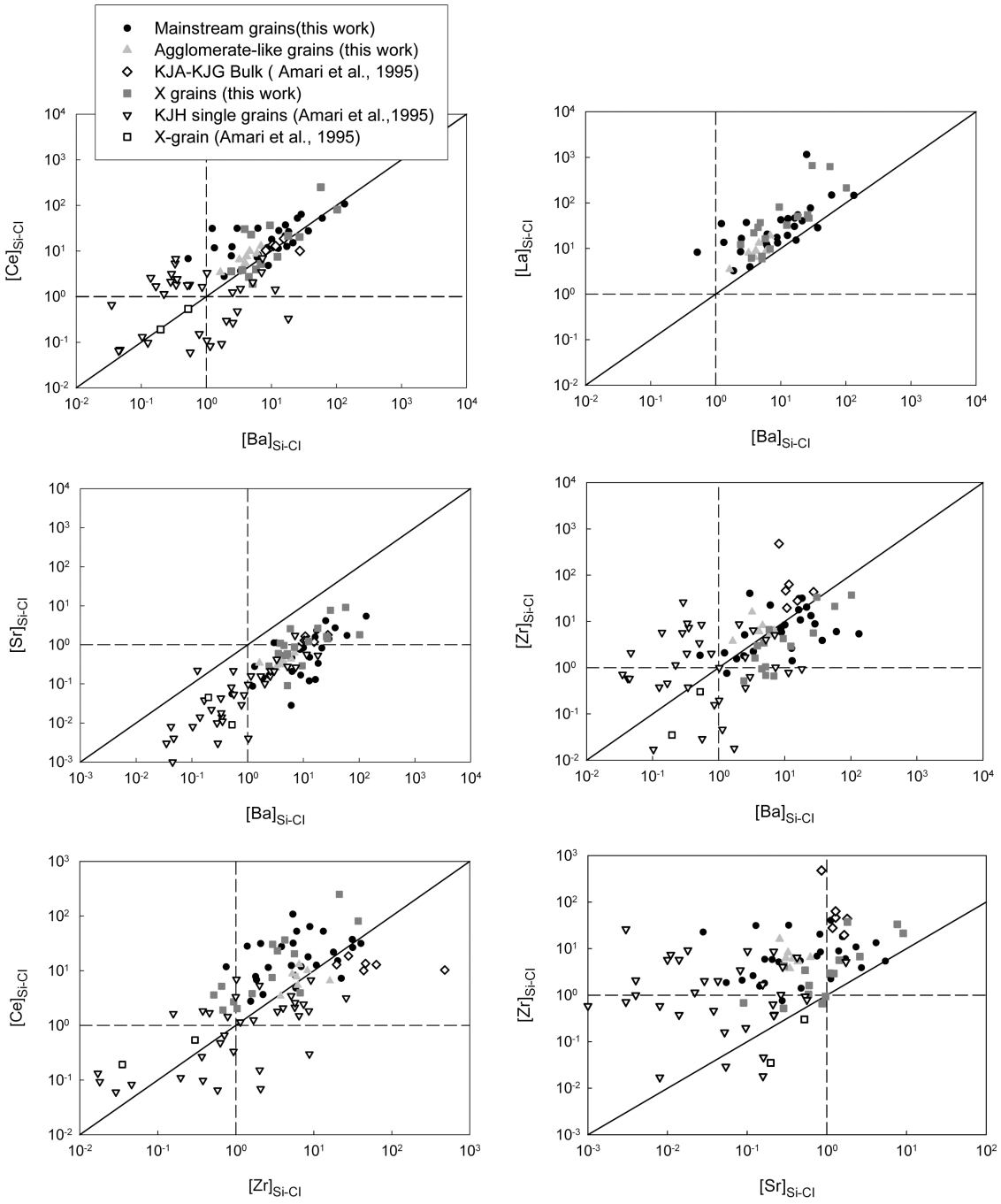

Fig. 6. Correlation plots for trace element abundances (normalized to Si and CI) for SiC agglomerate-like grains, mainstream grains and type X grains. For comparison data are plotted also for the fine grained KJA-KJG bulk samples and single KJH grains reported by Amari et al. (1995). Reasonably good correlations exist for [Ce]-[Ba], [La]-[Ba] and [Sr]-[Ba].

convective envelope penetrates into the upper layers of the helium intershell and mixes newly synthesized nuclei including *s*-process material to the stellar surface ("third dredge-up").

Key to the operation of the ^{13}C neutron source in AGB stars is the injection during each third dredge-up episode of a small amount of protons from the envelope into the top layers of the helium intershell. Within ~1000 years after the end of a third dredge-up event, a tiny ^{13}C pocket is formed by capture of these protons on ^{12}C via $^{12}C(p,\gamma)^{13}N(\beta^{+}\nu)^{13}C$. During the interpulse phase the ^{13}C pocket is compressed and heated. All ^{13}C nuclei burn via the reaction $^{13}C(\alpha,n)^{16}O$ in radiative conditions, at a temperature around 0.9×10^{8} K. This happens in less than 10,000 years, before the onset of the next thermal

pulse (Straniero et al. 1995). The maximum neutron density is low (~1 × 10^7 neutrons/cm^3). The other neutron source, ^{22}Ne, is activated during the thermal pulses and releases a second small neutron burst. ^{22}Ne is quite abundant in the He shell due to the conversion of the abundant ^{14}N from the CNO cycle via $^{14}N(\alpha,\gamma)^{18}F(,\beta^+\nu)^{18}O(\alpha,\gamma)^{22}Ne$. It becomes active during the convective thermal pulse at an average temperature of ~3 × 10^8 K and operates for a short time span of ~6 years. In low-mass AGB stars (1–3 $M_\odot$), the maximum neutron density is around 5 × 10^9 neutrons/cm^3. In intermediate mass AGB stars, where the peak neutron densities reach ~10^{11} neutrons/cm^3, contributions from the ^{22}Ne source are higher.

While most of the neutron exposure is due to operation of the ^{13}C source, the influence of the ^{22}Ne source clearly shows up at branchings, i.e., points in the *s*-process flow, where there is effective competition between neutron capture and β decay. A case in point is the branching at ^{134}Cs, which in turn governs the abundance of ^{134}Ba. The half-life of ^{134}Cs depends on temperature, decreasing at higher temperatures (2.06 years at room temperature; 308 days effective half-life at the temperature where the ^{13}C source operates, 32.7 days effective half-life at the temperature, where the ^{22}Ne neutron source operates; Takahashi and Yokoi 1987; Lugaro et al. 2003). While this favors decay to ^{134}Ba, and ^{134}Ba is in fact overproduced by ~50% with respect to ^{136}Ba during the ^{13}C source neutron flux, according to detailed calculations (Lugaro et al. 2003) during operation of the ^{22}Ne source the influence of the higher neutron density dominates over the increased decay rate, and ^{134}Ba is partially bypassed. The ^{136}Ba abundance, on the other hand, remains almost constant throughout the TP phase. Thus, in spite of the fact that both are pure *s*-process nuclides, one might expect to find variations in ^{134}Ba/^{136}Ba ratios, reflecting variations in the activation of the ^{22}Ne neutron source in the individual parent stars of the SiC grains. Additional small branchings occur at ^{135,136}Cs. Cesium-135 has a longer half-life of ~2 Myr (~1 Myr at the temperature where the ^{13}C source operates, and 1600 years at the temperature where the ^{22}Ne source operates), and, if ^{134}Ba is partly bypassed, ^{135}Ba is bypassed to the same extent. Cesium-136 has a short half-life of 13 days and mainly beta decays to ^{136}Ba, where the two *s*-process branches join. Only at very high neutron densities is ^{136}Ba also partly bypassed and ^{137}Cs accumulates during the short exposure in the thermal pulse, decaying to ^{137}Ba during the following interpulse phase (Lugaro et al. 2003).

Data obtained in previous analyses of "bulk SiC" (large agglomerates) by TIMS (Ott and Begemann 1990; Prombo et al. 1993) as well as SIMS (Zinner et al. 1991) have been found to fall on mixing lines between a component "N" (isotopically approximately normal material that is generally assumed to derive from the stellar envelope, but also including contamination) and a "G component" as synthesized in the *s*-process. In comparison with these earlier results, it is evident that for δ^{134}Ba versus δ^{135}Ba the average

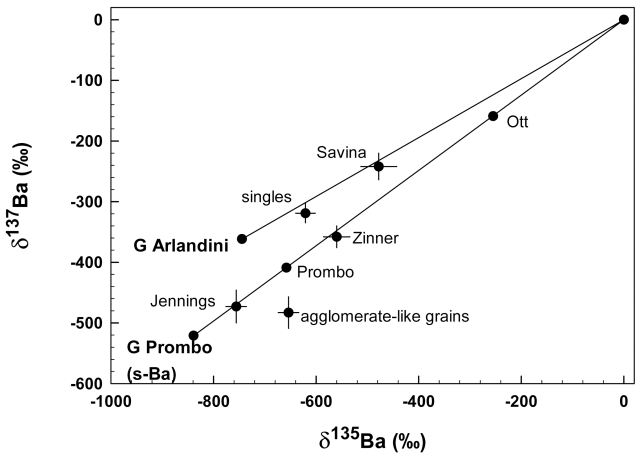

Fig. 7. Averages of Ba isotopic composition (^{137}Ba versus ^{135}Ba) for mainstream grains and agglomerate-like grains (this work) along with averages from previous work (as reported in Table 3). Also shown are mixing lines connecting normal Ba with *s*-process Ba derived by Prombo et al. (1993) and by Arlandini et al. (1999).

of our single grains plots on the mixing line defined by the N and G components and that for δ^{138}Ba versus δ^{135}Ba the average plots close to it (Figs. 5a and 5c). For δ^{137}Ba versus δ^{135}Ba, however, this is not the case, i.e., the single grain average plots above the mixing line (δ^{137}Ba is up by ~70‰) (Fig. 5b). As noted earlier, we cannot completely rule out an unidentified experimental bias (see discussion toward end of the Single Mainstream Grains and Agglomerate-Like Grains), but interestingly the agglomerate-like grains average shows just the opposite behavior, plotting below the G-N mixing line. This may be taken as an indication that the agglomerate-like grains rather than being large numbers of submicron-size grains in fact constitute a morphologically and isotopically distinct subpopulation of individual SiC grains. Such an interpretation would also be supported by a) the Si isotopes (Table 1; in particular the Z-grain-like shift of one of the aggregates noted at the beginning of the Single Mainstream Grains and Agglomerate-Like Grains section), b) their position in the Ba content versus grain size correlation (see discussion in the Source of Ba in SiC: Ion Implantation versus Condensation section), and c) the high-resolution NanoSIMS C isotope measurements made by Heck et al. (2007) on SiC grains with similar appearance.

We also note that in the δ^{137}Ba versus δ^{135}Ba representation, the mixing line between the N and the theoretical G component given by Arlandini et al. (1999) plots above the Prombo et al. mixing line (Fig. 7), roughly in agreement with our single grain average as well as the one for the Savina et al. (2003) single grains. For the latter we plotted a weighted average calculated from the individual data in their Table 1, which is different from the simple average the authors list in their Table 2.

The Ba isotopic compositions of SiC bulk samples and of single grains as measured by RIMS have been discussed in

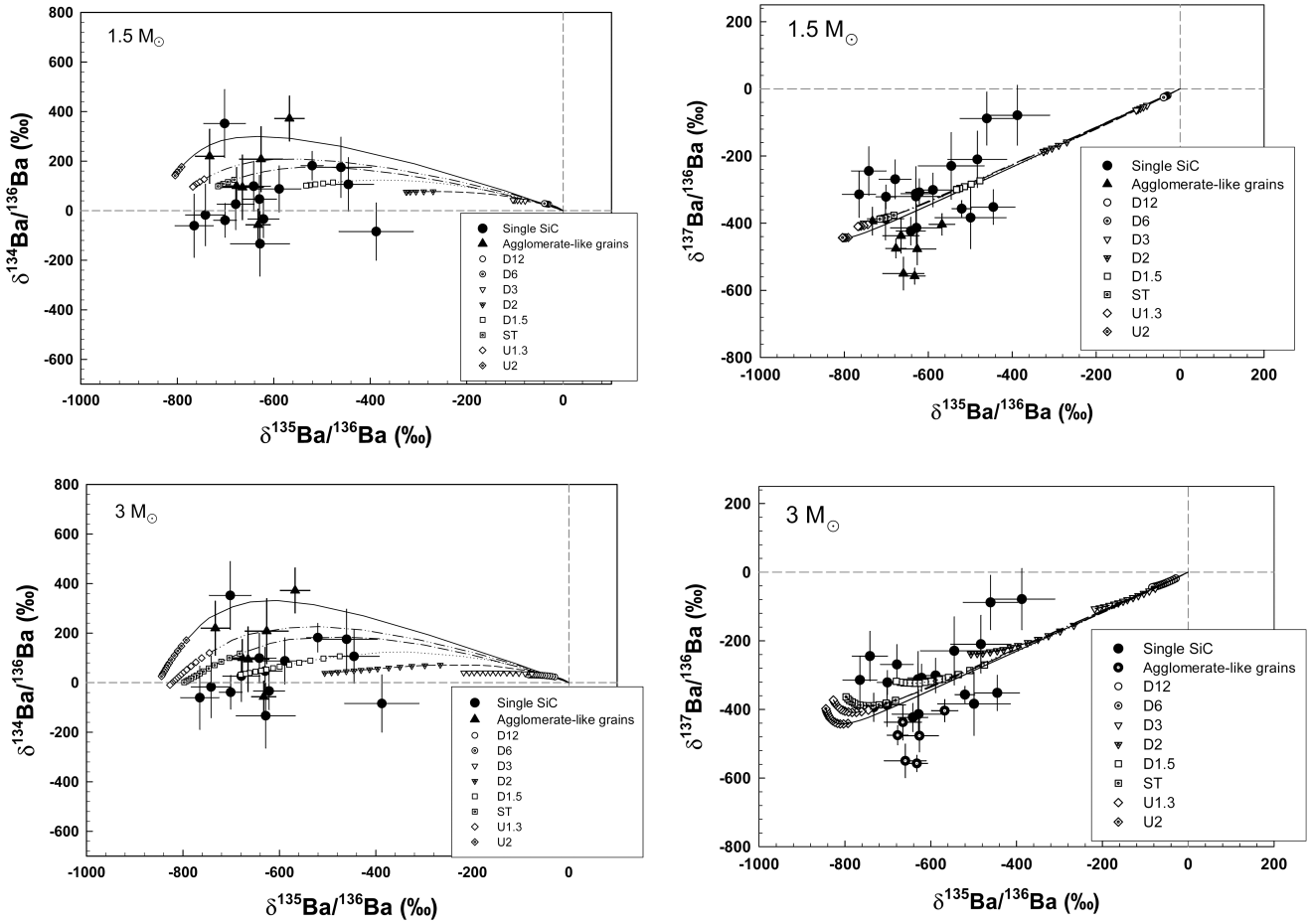

Fig. 8. Ba isotopic compositions of presolar SiC grains of this study in comparison with model predictions for 1.5 and 3 $M_\odot$ AGB stars with solar metallicity and varying ^{13}C pocket (courtesy A. Davis/R. Gallino). Symbols at the end of the model predicted lines indicate thermal pulses with C/O > 1.

terms of a variable ^{13}C pocket and stellar masses of 1.5, 3, and 5 $M_\odot$ by Lugaro et al. (2003) and Savina et al. (2003). The AGB star models have been termed according to the amount of ^{13}C present in the pocket, and models ranging from one-twelfth (D12) of the standard (ST) case to twice (U2) the ST case have been considered to explain the wide range of Ba isotopic compositions as measured by RIMS. Here the standard (ST) case for the ^{13}C pocket is defined as the one which, for a star of half solar metallicity, best reproduces the solar system *s*-process contribution (Gallino et al. 1998). Note that the model, except for the lower abundance of the metals relative to hydrogen, assumes elemental and isotopic abundance ratios that are solar initially. Note also that increasing/decreasing the amount of ^{13}C in the pocket is equivalent to decreasing/increasing the metallicity of the star. Hence, case U2 together with solar metallicity reproduces the solar system *s*-process abundance pattern as well. All the SiC data were explained using various AGB stars with masses between 1.5 and 3 $M_\odot$ with varying ^{13}C pocket, while a single AGB star with varying ^{13}C pocket covers only a very narrow range of the ^{13}C pockets that were earlier used to explain stellar observations. Besides low-mass (1.5–3 $M_\odot$) stars, Lugaro et al. (2003) have also discussed in detail the isotopic compositions of Ba from intermediate-mass (5 $M_\odot$) AGB stars. They also explored in detail the influence of the contribution from the ^{22}Ne neutron source, and, in addition, considered the effect on the final Ba isotopic composition of incorporating Cs into the SiC grains.

Figures 8a–c show the data measured in this work along with the model predictions for the case of 1.5 and 3 $M_\odot$ AGB stars of solar metallicity with different ^{13}C pockets. Our $\delta^{134}Ba$, $\delta^{135}Ba$, $\delta^{137}Ba$, and $\delta^{138}Ba$ values of many grains can be well explained by the predicted ranges of the models D1.5, ST, and U1.3 for M = 1.5–3 $M_\odot$. Barzyk et al. (2007), in their recent RIMS study, also reached a similar conclusion by removing the contaminated grains which were recognized in multi-element plots. Bonacic Marinovic et al. (2006) implemented *s*-process nucleosynthesis in stellar population calculations and showed that the *s*-process element distribution observed in stars of metallicity less than approximately one-tenth of solar can be explained by using only the models D1.5, ST, and U1.3, whereas previously

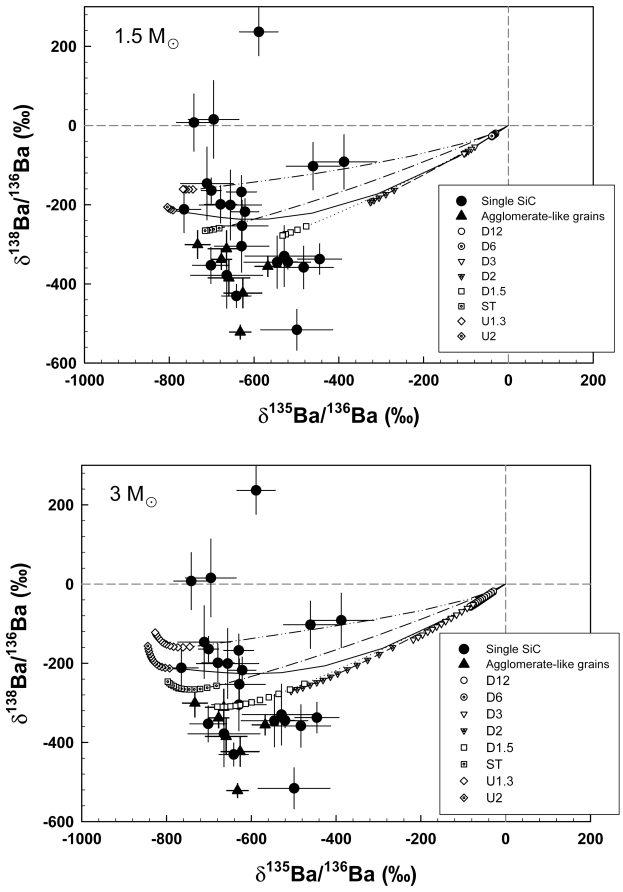

Fig. 8. *Continued.* Ba isotopic compositions of presolar SiC grains of this study in comparison with model predictions for 1.5 and 3 $M_\odot$ AGB stars with solar metallicity and varying ^{13}C pocket (courtesy A. Davis/R. Gallino). Symbols at the end of the model predicted lines indicate thermal pulses with C/O > 1.

Busso et al. (2001) needed models down to D24 to explain stellar observations and Lugaro et al. (2003) needed models down to D12 to explain presolar grains data. The new accurate data presented in this paper, together with the work of Barzyk et al. (2007) and Bonacic Marinovic et al. (2006) provide independent constraints for AGB star models, by reducing the needed ^{13}C spread from factors ~20 down to 2. Constraining the amount of ^{13}C can provide information on the complex physical processes that are supposed to drive the injection of protons into the He intershell, such as hydrodynamic overshoot, rotation, magnetic fields, gravity waves, which are difficult to model and are typically described using free parameters.

Notably, also in the $\delta^{137}Ba$ versus $\delta^{135}Ba$ plot, our data are rather symmetrically distributed around the predictions, which do not vary much in the range of interest in this case. For $\delta^{138}Ba$, however, there are several grains both at the high and low end that are much more extreme than predicted by any of the models. Currently we do not know whether certain parameters in the AGB star models could be adjusted in order to cover also the range of $\delta^{138}Ba$ seen in those grains. Qualitatively, higher ^{138}Ba abundances can be achieved by lower metallicities or higher ^{13}C amounts in the pocket but as far as we know there is no way to reproduce the most negative $\delta^{138}Ba$ values.

AGB stars of less than 1.5 $M_\odot$ are not expected to experience third dredge-up events (Karakas 2003) and can thus be excluded as stellar sources of presolar SiC. AGB stars with more than 5 $M_\odot$, on the other hand, are generally not expected to become enough carbon-rich to form SiC because of hot bottom burning (Boothroyd et al. 1993). Note, however, that according to calculations by Frost et al. (1998) some of the intermediate mass stars may become C-rich due to a rapid mass loss process called "super wind" leading to cessation of HBB. Anyhow, models for 5 $M_\odot$ AGB stars, in which ^{22}Ne is a highly efficient neutron source, show a strong enrichment in ^{137}Ba (Lugaro et al. 2003), which is not seen in any of our mainstream SiC grains.

Compared to the single grain data of Savina et al. (2003) our averages are more extreme, i.e., closer toward the *s*-process composition, in both $\delta^{137}Ba$ versus $\delta^{135}Ba$ and $\delta^{138}Ba$ versus $\delta^{135}Ba$. Many of their single grains lie very close to normal, solar Ba (N component), which was considered a puzzle by Savina et al. (2003) because: a) Zr and Mo isotopic analyses on a different set of grains showed that most of the grains contained >50% of G-component contribution in Zr and Mo (≤–500‰ for $\delta^{96}Zr$ and $\delta^{92}Mo$) (Nicolussi et al. 1997, 1998); and b) according to AGB star models it is expected that for grains where the G component contributes more than 50% to Zr and Mo also Ba has more than 50% G component contribution. This may be an indication of contamination in their study, e.g., due to impurities introduced during the chemical separation, presence of Ba-rich grains around the analyzed SiC grains, or Ba contamination in the gold substrate as discussed by Savina et al. (2003). In the present study, the advantage of using the NanoSIMS was the possibility to identify Ba contamination around the grains of interest and to exclude these grains from our study (Fig. 2) (see the Silicon and Barium Ion Imaging section). As a result, and in contrast to Savina et al. (2003), all grains in our study contain more than 50% G contribution in Ba and many plot very close to the G composition (Fig. 5).

In Fig. 9, we show $^{12}C/^{13}C$ ratios plotted versus $\delta^{135}Ba$ along with predictions for 1.5 and 3 $M_\odot$ AGB stars of solar metallicity with varying ^{13}C pocket. A weak correlation exists, similar to what is predicted by the models (higher $^{12}C/^{13}C$ for lower $^{135}Ba/^{136}Ba$). A similar correlation has been seen for grains measured by Savina et al. (2003). We note that, except for one X grain, the grain with $^{12}C/^{13}C = 10.8$—which could be an A/B grain—has the highest $^{135}Ba/^{136}Ba$ among the SiC grains of this study.

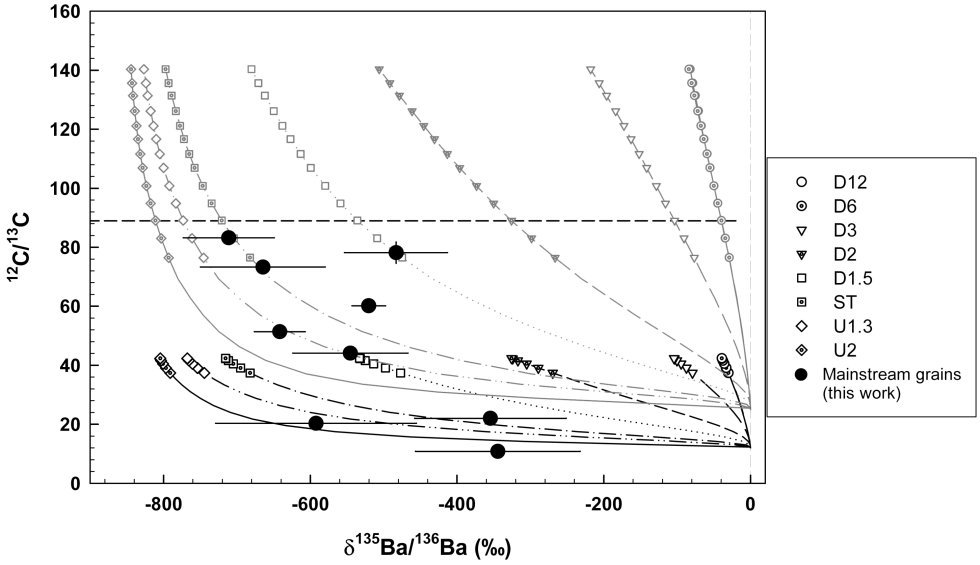

Fig. 9. $^{12}C/^{13}C$ versus $^{135}Ba/^{136}Ba$ for single SiC mainstream grains of this study. Model predictions for AGB stars are plotted for 1.5 $M_\odot$ (dark gray lines) and 3 $M_\odot$ (light gray lines) for comparison with varying ^{13}C pocket. A slight correlation exists between $^{12}C/^{13}C$ and $^{135}Ba/^{136}Ba$, as expected (see text).

X Grains, the *r*-Process, and Supernovae

Stringent constraints regarding the origin of Ba in X grains arise from our own data for three grains (Table 2). Data for an additional 6 grains reported in Pellin et al. (2000, 2006) do not include $^{134}Ba/^{136}Ba$. In addition, most have either large errors or compositions close to normal (indicative of possible contamination; see discussion in the previous section and Barzyk et al. 2007).

We first discuss a possible connection to the *r*-process. The importance of the *r*-process to the nucleosynthesis of the heavy elements has been known since 1957, when it was realized that it is responsible for about half of the heavy element solar system inventory beyond Fe (Burbidge et al. 1957; Cameron 1957). Its importance for research in meteoritics became apparent with the detection of ^{129}Xe excesses due to decay in early solar system materials of now extinct ^{129}I (Reynolds 1960); it became even clearer in the context of explaining the Xe-H component (Manuel et al. 1972) found in presolar nanodiamonds (Lewis et al. 1987).

In the *r*-process, the rate for neutron capture reactions is generally much higher than the respective beta decay rates of newly formed unstable n-rich isotopes. Stellar objects that can provide the required high neutron densities ($>10^{20}$ cm^{-3}) (Kratz et al. 1993), are core-collapse (type II) supernovae (SNe) and/or neutron stars during their merging with another neutron star or a black hole (NSMs) (see review articles by Qian 2003, 2005). Of the two, according to a detailed numerical study of the chemical evolution of our early galaxy (Argast et al. 2004), type II supernovae must be considered the major contributors to the *r*-process isotopes in the solar system.

The *s*-process is much better understood than the r-process, due to the fact that nuclear properties (nuclear cross sections and half-lives) of the nuclides in or close to the valley of β-stability are generally well known. Hence the solar r-process isotope abundances are traditionally calculated by subtracting the calculated solar *s*-process abundances from the observed solar abundances ($N_{r,\odot} = N_\odot – N_{s,\odot}$) (e.g., Kratz et al. 1993; Arlandini et al. 1999).

Returning to the X grains, the isotopic compositions of C, N, and Si and the presence of the decay products of short-lived nuclides such as ^{44}Ti ($T_{1/2}$ = 60 a) and ^{49}V ($T_{1/2}$ = 330 d) points toward type II SNe as the stellar source(s) (Amari et al. 1992; Nittler et al. 1996; Hoppe et al. 2000; Hoppe and Besmehn 2002). Hence, one might expect in SNe X grains enrichments in the *r*-process isotopes, i.e., mainly in ^{135}Ba, ^{137}Ba, and slightly in ^{138}Ba. Since ^{134}Ba and ^{136}Ba are not produced in the *r*-process, any event contributing an excess of *r*-process products should show maximum (relative) enhancement in $^{135}Ba/^{136}Ba$, and smaller enhancements of $^{137,138}Ba/^{136}Ba$, together with no effect on $^{134}Ba/^{136}Ba$. Data for our three X grains are not in agreement with these expectations as we see, relative to ^{136}Ba and normal composition, enrichments in ^{134}Ba and ^{138}Ba, coupled with depletions of ^{135}Ba and little effect on ^{137}Ba (Figs. 4 and 5).

The situation is illustrated in more detail in Figs. 10a–c, where the data are shown renormalized to ^{137}Ba and in absolute rather than δ-values. In the $^{134}Ba/^{137}Ba$ versus $^{136}Ba/^{137}Ba$ plot (Fig. 10a) our data fall slightly above a mixing line between *r*-process Ba ($^{134}Ba/^{137}Ba$ = $^{136}Ba/^{137}Ba$ = 0) and s-process Ba as produced in AGB stars (G component) (Prombo et al. 1993), although on both sides of isotopically normal Ba. In the $^{135}Ba/^{137}Ba$ versus $^{136}Ba/^{137}Ba$

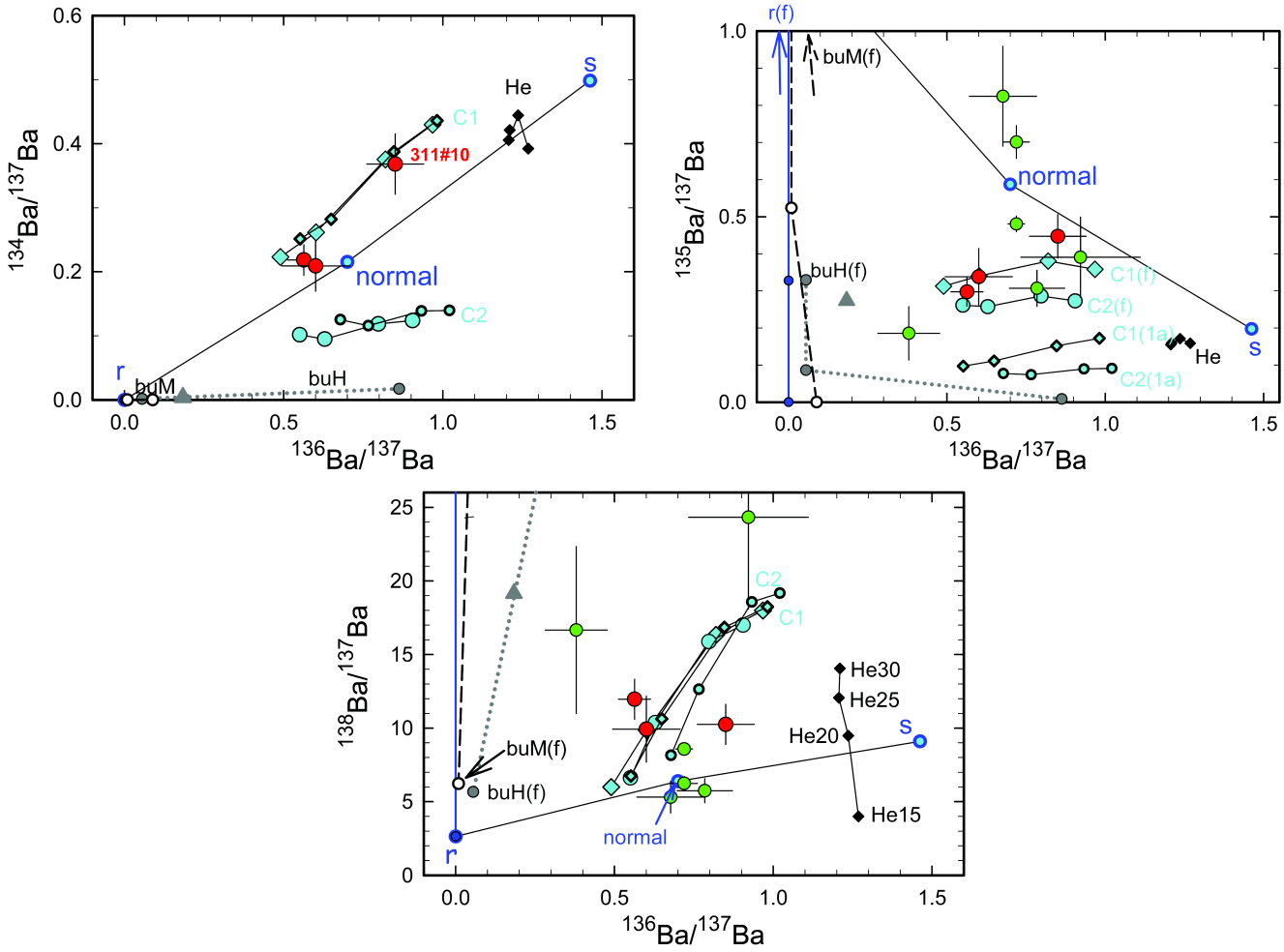

Fig. 10. Ba three-isotope plots for X grains normalized to ^{137}Ba. a) ^{134}Ba/^{137}Ba versus ^{136}Ba/^{137}Ba. b) ^{135}Ba/^{137}Ba versus ^{136}Ba/^{137}Ba. c) ^{138}Ba/^{137}Ba versus ^{136}Ba/^{137}Ba. Red data points = this work. Green data points = Pellin et al. (2000, 2006). All errors are 1σ. Also shown (blue) are normal Ba, *s*-process Ba, and *r*-process Ba as listed in Table 4. The compositions of neutron burst Ba (Table 4) according to Meyer et al. (2000) and Rauscher et al. (2002) are also shown, both at 1 year after SN explosion, 1 million years after SN explosion, and after complete decay of precursors (connected by lines). Blue line = *r*-process; dashed line (buM) = Meyer burst; gray dotted line (buH) = Heger-Rauscher burst. Final compositions (Table 4) are marked by "f" in some cases. Temporal changes in ^{136}Ba/^{137}Ba and ^{138}Ba/^{137}Ba are dictated by the time scale for decay of ^{137}Cs (half-life 30 years) and are virtually identical after 1 Myr and after complete decay. ^{138}Ba/^{137}Ba at one year is off scale. ^{135}Ba/^{137}Ba changes on a time scale also dictated by decay of ^{135}Cs (half life 2 Myr); final compositions for *r*-process and the Meyer n-burst are off scale. Gray triangles mark a mixture of 25% Heger-Rauscher burst after full decay of Cs precursors with 75% where Cs was separated from Ba after 1 year (see discussion in text). The compositions of weak *s*-process Ba produced during the first (labelled C1) and second (labelled C2) phase of shell C burning (see discussion in text) as predicted by Pignatari and Gallino for SN of different mass and solar metallicity are shown by the cyan diamonds and circles, respectively. Corresponding compositions at 1 year after explosion are shown as smaller symbols with black rim. Black diamonds labelled He show the Pignatari predictions for weak *s*-process during core He burning. There is little difference between early and final composition. Most obvious variations in weak *s*-process composition as a function of stellar mass are an increase with mass of ^{138}Ba/^{137}Ba for core He (as labelled; numbers refer to stellar masses), and of both ^{136}Ba/^{137}Ba and ^{138}Ba/^{137}Ba for shell C burning.

representation (Fig. 10b), our data as well as four out of the six grains of Pellin et al. (2000, 2006) are shifted from this mixing line toward lower ^{135}Ba/^{137}Ba and/or ^{136}Ba/^{137}Ba. The data may suggest a trend from a composition about midway between *s*-process and normal Ba to a point close to the origin in this representation. The enhancement of ^{138}Ba noted in Fig. 5c is also clearly visible in the ^{137}Ba normalized representation of Fig. 10c for our as well as some of the Pellin et al. X grains, with their other grains being normal within error. Clearly, in none of the plots is there a shift evident as expected from simple addition to normal Ba of *r*-process material with ^{136}Ba/^{137}Ba = 0.

A possible explanation for depletions relative to normal (or lack of enrichments with respect to *s*-process abundances) of ^{135}Ba and ^{137}Ba could be the relatively long half lives of the radioactive ^{135}Cs and ^{137}Cs precursors (2 Myr and 30 years, respectively), which serve as shields in the *r*-process. This is because a) cesium is a volatile element and not expected to

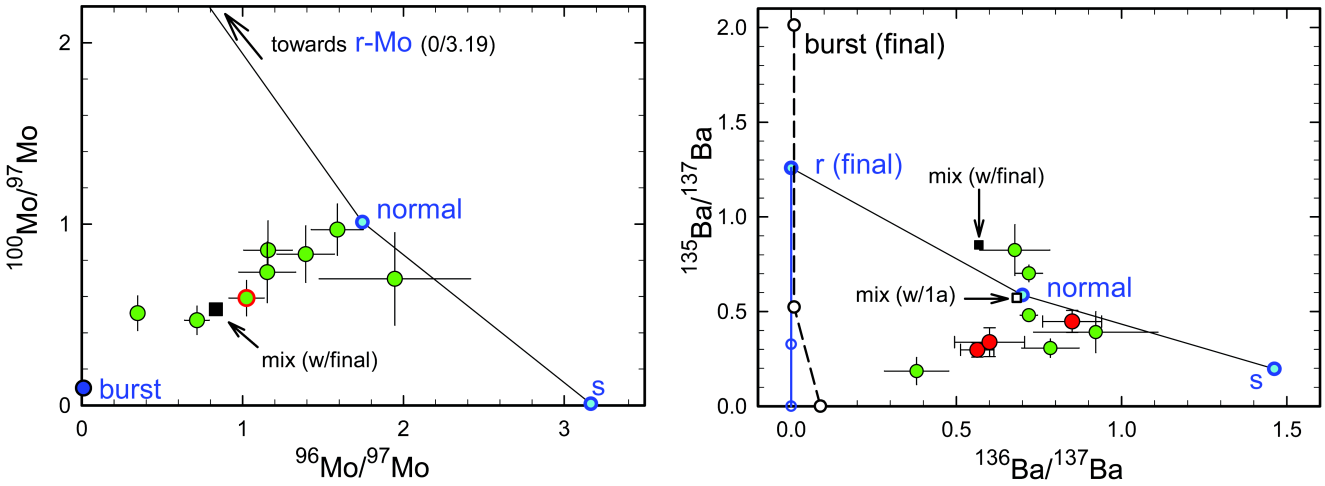

Fig. 11. Comparison of "simple" situation in molybdenum with more complex situation in barium. a) In a three-isotope plot ^{100}Mo/^{97}Mo versus ^{96}Mo/^{97}Mo data (from Pellin et al. 2006) plot on a mixing line between isotopically normal (solar) Mo and n-burst Mo (Meyer et al. 2000; see http://nucleo.ces.clemson.edu/pages/tables/tables_data/final.mass_lpsc31.dat) plotting close to the origin. b) The same mixture does not explain the Ba data as shown in a plot ^{135}Ba/^{137}Ba versus ^{136}Ba/^{137}Ba, neither using the final n-burst composition after full decay of precursors, nor at earlier times.

condense into SiC, and b) from a Ti-V study of X grains it appears that X grains condense from supernova ejecta within a year or so of the explosion (Hoppe and Besmehn 2002). Note that a similar time scale for dust formation around supernovae type II is suggested by spectroscopic observations of SN 1987a (e.g., Haas et al. 1990; Kosaza et al. 1991). Hence ^{135}Cs and ^{137}Cs shielding would be a plausible mechanism to keep ^{135}Ba and ^{137}Ba abundances low, while allowing for strong enrichment of ^{138}Ba. In this case, the ratio of these two isotopes relative to ^{136}Ba in the mixture would remain essentially unaffected by the *r*-process contribution simply because so little would be added. The argument, of course, does not hold if Ba and Cs would be implanted rather than condensed into the grains (see the Source of Ba in SiC: Ion Implantation versus Condensation section). It would also not allow explaining the observed compositions by mixing r-process matter with isotopically normal Ba, since it could not arrive at a composition that has higher ^{136}Ba/^{137}Ba than solar system Ba.

The observed Ba isotopic patterns in X grains are not the only ones inconsistent with expectations for a simple r-process + normal mixture. Similar problems have been encountered with Mo and Zr (Pellin et al. 2000, 2006). The observed excesses relative to ^{96}Mo (pure *s*-process product) of ^{95}Mo and ^{97}Mo without corresponding enrichment in ^{100}Mo (pure *r*-process product) cannot be explained by addition to solar of unadulterated *r*-process material (Fig. 11a). Note that in this case no long-lived precursor is involved so that even elemental fractionation like between Ba and Cs does not offer a way out. As for Zr, the isotopic pattern (dominated by a large enrichment in ^{96}Zr) is incompatible with the expectations for addition of classical *r*- or *s*-process Zr to normal Zr. Another similar case is that of Xe-HL in presolar diamonds (e.g., Ott 1996), where addition of *r*-process Xe should lead to equal (percentage-wise) enhancements of the two r-only isotopes ^{134}Xe and ^{136}Xe, contrary to observations. In order to explain these patterns, a special scenario of a short-neutron burst has been invoked (Meyer et al. 2000), which we will discuss in the following section, together with other possibilities.

Neutron Bursts, Weak *s*-Process, and Other Alternatives

A neutron "burst" (intermediate between the common s- and *r*-processes) was first considered by Heymann and Dziczkaniec (1979) in order to explain the Xe-H part of the Xe-HL signature found in presolar diamonds. The most likely astrophysical environments for this process, as for the r-process, are type II SN explosions. Two specific sites have been proposed: explosive carbon burning near the base of the C-burning shell (Heymann and Dzickaniec 1979) and the expanding He shell at the time the shock wave passes through (Clayton 1989; Howard et al. 1992; Meyer et al. 2000).

Meyer Neutron Burst

In the current context, the short neutron burst within the shocked He-rich matter in an exploding supernova (Meyer et al. 2000) is especially relevant because it appears to offer an explanation for the strange isotopic patterns of Mo, Sr, and Zr isotopes in X grains (Pellin et al. 1999, 2000, 2006; Meyer et al. 2000). In addition, as originally intended (Clayton 1989) the burst may also explain the composition of Xe-H in the presolar diamonds. As shown by Ott (2002), mixing of 83% of solar matter $N_{\odot}$ and 17% of Meyer's neutron burst matter $N_{n\text{-burst}}$ gives a reasonably good agreement with the Mo pattern observed by Pellin et al. (2000, 2006) in SiC X grain

Table 4. Ba isotopic composition measured in SiC from the Murchison meteorite in this work and by Pellin et al. (2000, 2006) in comparison with normal Ba and model predictions for various components in massive stars.

Study	Sample	^{134}Ba /^{137}Ba	^{135}Ba/^{137}Ba	^{136}Ba/^{137}Ba	^{138}Ba/^{137}Ba
Pellin et al. 2000, 2006	113-2		0.391 ± 0.108	0.922 ± 0.188	24.32 ± 6.23
	113-3		0.185 ± 0.072	0.380 ± 0.097	16.66 ± 5.67
	153-8		0.825 ± 0.135	0.677 ± 0.108	5.31 ± 1.07
	133-1		0.480 ± 0.021	0.719 ± 0.026	8.57 ± 0.40
	327-5		0.701 ± 0.044	0.719 ± 0.041	6.24 ± 0.46
	032-2		0.307 ± 0.048	0.784 ± 0.087	5.74 ± 0.81
This work	629#2	0.219 ± 0.031	0.297 ± 0.047	0.563 ± 0.051	11.97 ± 1.35
	373#3	0.209 ± 0.054	0.338 ± 0.097	0.600 ± 0.106	9.93 ± 2.24
	311#10	0.368 ± 0.061	0.447 ± 0.075	0.850 ± 0.090	10.25 ± 1.36
AGB *s*-process (Prombo et al. 1993)		0.499	0.197	1.46	9.093
Normal (Lewis et al. 1983)		0.2155	0.5873	0.6997	6.388
r-process (Arlandini et al. 1999)		0 (–, 1)	1.259 (1, 1)	0 (–, 1)	2.64 (0, 1)
n-burst (Meyer et al. 2000)[a]		2.51×10^{-7} (0.872, 0.918)	2.013 (1.000, 0.918)	0.00911 (0, 0.918)	6.23 (0, 0.918)
n-burst (Rauscher et al. 2002)[b]		0.00163 (0.458, 0.958)	0.329 (0.998, 0.958)	0.0550 (0, 0.958)	5.66 (0, 0.958)
Weak He core (Pignatari and Gallino)[c]	20 $M_\odot$	0.444 (0, 0.000)	0.171 (0.015, 0.000)	1.236 (0, 0.000)	9.478 (0, 0.000)
Weak C shell (Pignatari and Gallino)[c]	(1st) 20 $M_\odot$	0.262 (0, 0.075)	0.340 (0.698, 0.075)	0.602 (0, 0.075)	9.857 (0, 0.075)
Weak C shell (Pignatari and Gallino)[c]	(2nd) 20 $M_\odot$	0.095 (0, 0.183)	0.257 (0.764, 0.183)	0.629 (0, 0.183)	10.38 (0, 0.183)

[a]Model predictions data: http://nucleo.ces.clemson.edu/pages/tables/tables_data/nburst_lpsc31.dat and http://nucleo.ces.clemson.edu/pages/tables/tables_data/final.mass_lpsc31.dat.

[b]Model prediction data at www.nucleosynthesis.org. (O/C region, ~5.6–7.1 solar mass from the central core of the 25 solar mass.)

[c]Predictions by Pignatari and Gallino for weak *s*-process during He core and C shell burning: private communication; exemplary values for 20 solar mass star of solar metallicity (see text for further discussion).

Where significant contributions to the final abundances of the Ba isotopes are held up in ^{134}Cs (half life 2.06 yr), ^{137}Cs (30 yr), or ^{135}Cs (2 Myr), the corresponding fractions are given in parentheses: isotope in the nominator (first) and denominator (second).

113-2 (cf. also Table 4) as well as with the Xe-H pattern. The case for Mo is demonstrated in Fig. 11a, which is a three-isotope plot ^{100}Mo/^{97}Mo versus ^{96}Mo/^{97}Mo of the Pellin et al. data. Obviously all measured compositions are well explained by a normal + neutron burst mixture. The specific grain 113-2 is marked by a rim around the symbol and is quite typical. The composition of the calculated mixture is shown by the black square. Plots such as Fig. 11a involving the r-only isotope ^{100}Mo (almost no production in the n-burst) allows to distinguish between n-burst and *r*-process as the one endmember, In plots involving only the other Mo isotopes, the data are equally well explained by a mixture of normal and *r*-process Mo. Ott (2002) also suggested that the n-burst may be the recently inferred "weak" *r*-process (e.g., Sneden et al. 2000) or a part of it and that it may have made a significant contribution to the heavy elements in the solar system.

In Table 4 we list the Ba isotopic patterns according to Meyer's predictions (http://nucleo.ces.clemson.edu/pages/tables) along with the *r*-process and other relevant compositions. All compositions are given after full decay of unstable precursors. In addition, we list (in parentheses) the fractions that are held up at radioactive Cs precursors: ^{134}Cs (half life 2.06 yr), ^{135}Cs (2 Myr), and ^{137}Cs (30 yr). All compositions are also shown in Figs. 10a–c. There is *r*-process like close to zero production of ^{134}Ba and ^{136}Ba. After one year, which may approximate the time of grain condensation (see the X Grains, *r*-Process, and Supernovae section), ^{138}Ba and that little predicted ^{136}Ba are fully present and a significant fraction of the tiny amount passing through ^{134}Cs has decayed into ^{134}Ba. Mass 135 and 137 precursors are largely held up in ^{135}Cs and ^{137}Cs, respectively. At 1 Myr, decay of ^{137}Cs is complete, while decay of ^{135}Cs only starts to show up. It is obvious, in any case, that—independent of time—the trend predicted by mixing normal and Meyer neutron burst material does not agree with what is observed. Most crucial, not only does the model predict significant overproduction (relative to ^{136}Ba) of ^{138}Ba, but also of ^{137}Ba and for late grain formation (or no Cs/Ba separation) of ^{135}Ba, which is not seen. Nor is there strong evidence observed for the predicted depletion of ^{134}Ba (Fig. 10a; Table 4); in fact, one of our grains shows strongly enhanced ^{134}Ba/^{137}Ba.

For a quantitative comparison, we have applied the mixing scheme used by Ott (2002) in order to explain Mo in X grain

113-2 (Fig. 11a) as well as Xe-H in presolar diamond, i.e., 83% of $N_{\odot}$ and 17% $N_{n\text{-}burst}$. The resulting composition is shown in the $^{135}Ba/^{137}Ba$ versus $^{136}Ba/^{137}Ba$ plot of Fig. 11b as an open square (using n-burst composition after 1 yr) and as a full square (after complete decay). Note that for Mo and Xe (except for ^{129}Xe), precursors have half-lives much shorter than 1 year so that it is not necessary to make the distinction for these elements. Although there is also some noticeable direct production of ^{137}Ba and also of a little ^{134}Ba (on the order after one-tenth of the already small total), contributions after one year are too small to cause any significant deviation from normal composition, while after full decay trends go into the wrong direction. Quite obviously, the case of Ba is significantly more complex than that of Mo (and Zr, for that matter).

Other Neutron Bursts

As discussed by Davis (2004), a neutron burst is also clearly seen in the supernova explosion models given by Rauscher et al. (2002). In their models for a 25 $M_{\odot}$ star, the neutron burst occurs in the outer O/C region (around 6.5–7.1 $M_{\odot}$ from the central core of the supernovae, below the helium shell). Barium isotopic compositions from their ("Heger-Rauscher") nucleosynthesis calculations for this zone (see http://www.nucleosynthesis.org) are also listed in Table 4 and shown in Figs. 10a–c, again after 1 yr, 1 Myr, and complete decay. There are some differences in the detailed predictions (Table 4), in particular in the $^{135}Ba/^{137}Ba$ ratio, which is significantly higher in the Meyer burst. Nevertheless, qualitatively the behaviors are similar: a) both burst models can explain the enhanced ^{138}Ba abundance, b) in the ^{135}Ba-^{136}Ba-^{137}Ba-^{138}Ba system, data may be marginally compatible with a mixture of normal and some neutron burst material of the Heger-Rauscher type if augmented by Cs/Ba separation; early separation of Cs, however, may cause problems in quantitative terms, and c) in detail, simple mixing with Ba of normal composition, in whatever ratio, cannot result in the full set of measured compositions: this is obvious when ^{134}Ba in grain 311#10 is involved, as shown in Fig. 10a, where $^{134}Ba/^{137}Ba$ is plotted on the ordinate. The burst models predict way too little ^{134}Ba in order to match the observed compositions by mixing with normal Ba; in particular, in no way can they result in the enhanced $^{134}Ba/^{137}Ba$ seen in this grain (Fig. 10a).

Weak s-*Process*

Another process acting in massive stars and contributing by neutron capture to nucleosynthesis of the heavy elements is the weak *s*-process. The weak *s*-process dominates over the *s*-process main component in the mass range below A ~90 in the solar system distribution (e.g., Käppeler et al. 1989) and is thought to occur in massive stars most likely during core He and/or shell C burning (e.g., Raiteri et al. 1993). Latest results of dedicated calculations for solar metallicity stars of 15, 20, 25, and 30 solar masses by Pignatari and Gallino (M. Pignatari, personal communication) are included in Figs.10a–c. Results for the 20 solar mass case are also listed in Table 4. Three settings/cases are shown: results for weak s-process during core He burning (labelled He in Fig. 10) as well as two phases (labelled C1 and C2) during shell C burning. Phase C1 operates in the convective C shell at an almost constant temperature 1.0 to 1.15×10^9 K, C2 in the last moments before the explosion, when oxygen and Si are burning in deeper layers (Pignatari, personal communication). Details of phase 2 and whether it happens at all are model-dependent. In contrast to the *r*-process and the neutron bursts, the weak *s*-process operates on a significantly longer time scale (years for shell C burning phase 1, even longer for core He burning). Also, there is generally not much contribution from decay of radioactive precursors after the process, and only for ^{135}Ba in shell C burning (to some extent also for ^{137}Ba from phase C2) is there a noticeable difference between various times shown in Figs. 10a–c.

The plots of Fig. 10 show that mixture of Pignatari weak *s*-process from core He burning and normal Ba is unable to reproduce the Ba isotopic pattern seen in the X grains data either. On the other hand, predictions from C shell burning, especially phase 1, are quite similar to our measured values. We believe this to be fortuitous and not to indicate such Ba to be the dominant contributor to Ba in the grains. For one, this would require almost pure Ba of this type to be present, which appears highly unlikely. Further, we have obtained predictions for Ba from the weak *s*-process for the mass range 15–30 solar masses by L.-S. The (The et al. 2007), and we also extracted relevant data from the Heger-Rauscher model (Rauscher et al. 2002; http://www.nucleosynthesis.org). These are excluded from Fig. 10 so as not to clutter this already complicated figure. However, inspection of the various data sets shows quite significant differences between predictions from the different workers indicating a strong model dependency. While the Heger-Rauscher predictions for *s*-process during core He burning are similar to those of Pignatari/Gallino, those from The et al. are characterized by much lower $^{136}Ba/^{137}Ba$ and $^{134}Ba/^{137}Ba$ ratios. Their predictions for C shell weak *s*-process are quite similar. As for differences in C shell predictions between Heger-Rauscher and Pignatari/Gallino, the former are primarily characterized by lower $^{134}Ba/^{137}Ba$ and $^{138}Ba/^{137}Ba$. In any case, the strongest argument against a dominant weak *s*-process contribution comes from the existing Mo data (cf. Fig. 11a). In Mo, the weak component is characterized not only by absence of r-only ^{100}Mo (which would be consistent with the data), but also by strong enhancement of s-only ^{96}Mo (Rauscher et al. 2002), with $^{96}Mo/^{97}Mo$ approaching the ratio in the main component from AGB stars. For this there is no evidence whatsoever in the grain data (Fig. 11a).

More Components

The major problem in our attempts above to identify some type of neutron burst (or *r*-process, if it were not for the

Zr/Mo situation) as contributor to the Ba isotopes in the X grains may lie in our assumption of a two-component mixture, with one of the components being isotopically normal (solar-type) Ba. The situation changes, if we relax this boundary condition. If a third *s*-process-rich/like component contributes, the data allow also for contributions from a neutron burst. The high $^{138}Ba/^{137}Ba$ in this case is suggestive for the n-burst component to have experienced a Cs/Ba fractionation event (during condensation?) on a time scale of very roughly 10 (Meyer's n-burst ratio ~23) years after supernova explosion. This is considerably longer than the time scale inferred from V-Ti (Besmehn and Hoppe 2002).

The shorter time scale is not excluded if the errors (1σ in the tables) of the Ba isotopic ratios are considered. But they may also indicate that part of the trace elements were introduced without strong fractionation, e.g., by ion implantation. This situation would be similar to that suggested for the trace elements in mainstream SiC from AGB stars (Verchovsky et al. 2004; Yin et al. 2005; see the following section). Using the nominal data some 25% of unfractionated material would be needed to achieve agreement in $^{138}Ba/^{137}Ba$ (Fig. 10c). For the Heger-Rauscher neutron burst the resulting composition (gray triangle in Fig. 10) would also be consistent in $^{134}Ba/^{137}Ba$ and $^{135}Ba/^{137}Ba$ versus $^{136}Ba/^{137}Ba$. For the Meyer neutron burst, on the other hand, the resulting $^{135}Ba/^{137}Ba$ would be much too high (offscale in Fig. 10b), reflecting the more than 6× higher predicted $^{135}Ba/^{137}Ba$ ratio after full decay (Table 4). Obviously, more reliable predictions for neutron burst Ba are needed before any reliable conclusions are possible. Note that a similar problem does not exist in the "simple case" of Mo (Fig. 11a). The additional *s*-process contribution in our three-component mixing scheme may be a separate component, e.g., the weak component(s) discussed above. While in such a scenario the mixing ratio, of course, is a free parameter, it is instructive, nevertheless, to consider here if sufficient weak s-process Ba is present in the parent massive stars of the X grains. Judging from the data for the Heger-Rauscher 25 solar mass model, there well may be enough, with a rough figure for weak *s*-process ^{137}Ba/neutron burst ^{137}Ba being ~0.4.

Alternatively the *s*-process rich Ba may be present in the form of "normal" Ba that is more *s*-process rich than solar Ba, i.e., it may be part of the Ba inherited by the star upon its formation, having been preserved in its envelope. We note that this would be contrary to expectations from simple models of galactic chemical evolution, where the ratio of s/r products is expected to steadily increase with time. The parent stars of the SiC-X grains, being massive stars, would not have lived very long, thus being close in formation age to the Sun; the expected s/r ratio would be similar to solar. Nevertheless, observations show that there is actually scatter of individual stellar compositions around an average evolution (e.g., Mathews et al. 1992), and the ~25% enhancement needed here (corresponding to $^{136}Ba/^{137}Ba$ ~0.9; cf. Fig. 10) is well within this scatter. Hence, we conclude that there is no a priori

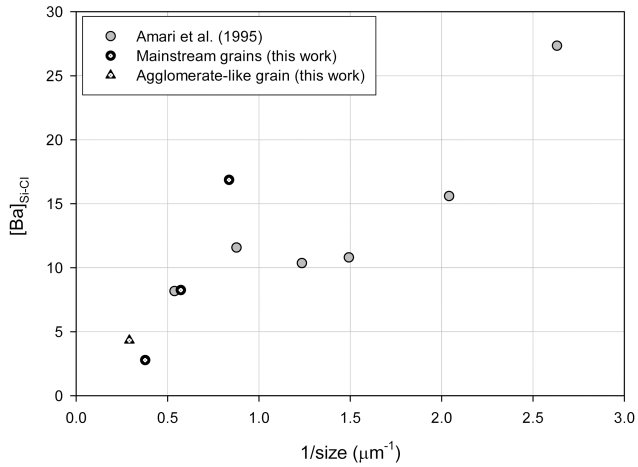

Fig. 12. Average Ba concentration (normalized to Si and CI) versus inverse grain size for SiC agglomerate-like grains and single mainstream grains. To reduce scatter, the 26 mainstream grains were divided into three different size bins for which three average Ba concentrations were calculated, while for the agglomerate-like grains the mean is plotted. Data from Amari et al. (1995) are shown for comparison. The positive correlation between Ba concentration and inverse grain size indicates a contribution from ion implantation.

reason why envelope Ba should have exactly the same isotopic composition, i.e., same mixing ratio of *s*- and *r*-process as solar Ba. Nor is there a reason why various parent stars of individual grains should have identical mixing ratios.

Summing up the X Grains, the *r*-Process, and Supernovae section and the Neutron Bursts, Weak *s*-Process, and Other Alternatives section, we conclude that mixing of *r*-process or neutron burst Ba with isotopically normal (solar-system) Ba cannot account for the Ba isotopic composition observed in the X grains. Invoking a third *s*-process rich component (e.g., from the weak *s*-process in the parent star) or having an envelope component more *s*-process rich than solar Ba may do the trick, if, in addition n-burst Ba is affected by Cs/Ba fractionation ~10 years after supernova explosion. An alternative to delayed separation/incorporation would be separation/incorporation at ~1 year (as indicated from other evidence) augmented by introduction of a fraction (on the order of one-fourth) of unfractionated neutron burst matter, if the yields from the Heger-Rauscher calculations are used. The scheme would not work, however, with the Meyer neutron burst predictions, indicating the need for more reliable calculations of neutron burst nucleosynthesis in difficult cases like Ba. Also, while massive stars and low-mass stars should behave the same in this respect, there is no evidence in SiC from AGB stars for a scatter in their initial composition, which might appear to be a problem for the variations considered for the parent stars of the X grains. The data are not conclusive, however. Now that data points close to the origin in the delta plots of Figs. 5 and 8 have been shown to be affected by contamination (see discussion in the Mainstream Grains and *s*-Process Nucleosynthesis of Ba in AGB Stars section; and Barzyk et al. 2007) it appears difficult to rule out

a scatter in envelope/"normal" composition commensurate with that envisioned for the X grains. Further experimental and theoretical work will be needed to pin down the origin of n-capture trace elements in SiC X grains.

Source of Ba in SiC: Ion Implantation versus Condensation

On the basis of an inferred Ba/Xe ratio in SiC of around 1800, Ott and Begemann (1990) suggested that Ba may have been trapped by implantation just as the noble gases are believed to have been. On the other hand, Zinner et al. (1991), who found an ~10× higher Ba-S/Xe-S ratio favored the co-condensation of refractory elements like Ba into SiC. Condensation calculations (Lodders and Fegley 1995, 1997) show that Ba may indeed condense into SiC as BaS.

In Fig. 12, we have plotted the Ba concentration as a function of inverse grain size for the mainstream grains (binned to reduce scatter) of this study. For comparison, we have also included the KJH grains measured by Amari et al. (1995) and the average of the seven agglomerate-like grains. There is a correlation, which is roughly compatible (within uncertainties) with a 1/r dependence. Notably, the agglomerate-like grains plot at a position consistent with their true size and not at the position expected if they were composed of submicron grains. This may be taken as an indication that they rather constitute a separate population of SiC grains, for which there is also indication in the Ba and Si isotopic compositions (see discussion in the Mainstream Grains and *s*-Process Nucleosynthesis of Ba in AGB Stars section).

With La/Ba, Ce/Ba, and Sr/Ba essentially constant (Fig. 6), the situation is similar also for these correlated elements. This seems to indicate that some non-negligible fraction of Ba (and other trace elements) was implanted into the mainstream SiC grains. In fact, Verchovsky et al. (2004) and Verchovsky and Wright (2004) have proposed that up to ~60% (for the finest fractions) of the Ba in SiC was trapped by ion implantation and that the rest had been co-condensing into the SiC grains. Also, Yin et al. (2006), based on the abundance pattern in the Ba to Hf range obtained on bulk SiC by ICP-MS, argued for a major ion implantation contribution to Ba. These authors observed the refractory rare earth elements to be present in abundance ratios close to production ratios, but the more volatile REE (Sm, Eu, Yb) to be depleted. Since Ba was less depleted than the volatile REE, but was expected to condense into SiC at even lower temperature they suggested that the difference was made up by ion implantation that favored Ba over the REE.

Implantation would have resulted in the effective incorporation of easily ionized Cs and the shielding effect discussed in connection with the Ba isotopic data of the X grains (see the X Grains, the *r*-Process, and Supernovae section and Neutron Bursts, Weak *s*-Process, and Other Alternatives section) would not work. However, although there are no clear differences in abundances, the processes by which Ba and other trace elements were incorporated in mainstream grains and X grains, which formed from very different stellar sources, may have been quite different. Clearly, more isotopic and abundance data are needed in order to get a more profound understanding of the trapping mechanisms for trace elements into various types of presolar SiC grains.

SUMMARY

We have measured the Ba isotopic compositions of single presolar SiC grains and agglomerate-like grains by NanoSIMS. Our studies comprised 26 (likely) mainstream grains (0.8–2.6 μm), 19 X grains (0.2–2.3 μm), and 7 agglomerate-like grains (1.2–5.3 μm). The most important results can be summarized as follows:

1. Ba isotopic measurements are feasible by NanoSIMS for single grains with sizes between <1 and 3 μm. Except for the very rare p-only ^{130}Ba and ^{132}Ba, all other isotopes were included in our measurements.
2. The agglomerate-like grains and (likely) mainstream grains are characterized by typical *s*-process patterns with lower than solar ^{135,137,138}Ba/^{136}Ba and close-to-solar ^{134}Ba/^{136}Ba. The observed Ba isotopic ratios of most grains are well explained by models for 1–3 $M_{\odot}$ AGB stars with varying ^{13}C pocket. The new accurate data presented in this paper provide independent constraint for AGB models, by reducing the needed ^{13}C spread from factors ~20 down to 2. Some of the grains exhibit ^{138}Ba/^{136}Ba ratios lower or higher than predicted. This suggests that the explored parameter space in current AGB star models may have to be extended.
3. Differences between agglomerate-like grains and single grains as well as the Ba concentration of the agglomerate-like grains may indicate that rather than being composed of typical submicron-sized grains the agglomerate-like grains represent a separate grain population.
4. Because of small grain size and/or low Ba concentrations, useful isotope data could be obtained only for 3 X grains. All exhibit excesses in ^{134}Ba and ^{138}Ba and compared to mainstream grains they also have relative enrichments in ^{135}Ba and ^{137}Ba. The observed signature cannot be explained by mixing of either r-process or neutron burst Ba with Ba of solar composition. The observed signature could indicate a mixture of a) "normal Ba" more *s*-process rich than solar, or b) normal Ba plus weak *s*-process Ba, with n-burst type Ba where Cs was separated from Ba, possibly ~10 years after SN explosion. Depending on the n-burst predictions, this scheme works for Heger-Rauscher only (Rauscher et al. 2002; http://www.nucleosynthesis.org), not for Meyer's predictions (Meyer et al. 2000). Another possibility is early separation (at ~1 year) coupled with

addition of some fraction (on the order of one-fourth) of unfractionated n-burst matter. Due to large analytical uncertainties and conflicting theoretical predictions, it is difficult to come up with a unique solution, however. More work, both experimentally and theoretically, will be required to identify the origin of Ba in SiC X grains.

5. For the mainstream grains there is an anti-correlation between Ba concentration and grain size. This is taken as an indication that some of the Ba was trapped by ion implantation.

Acknowledgments–We thank Joachim Huth for his help with the SEM, Christa Sudek for her help with the chemical separation of presolar grains, and Elmar Gröner for technical assistance on the NanoSIMS. We also thank Roberto Gallino and Marco Pignatari for discussion of the *s*-process nucleosynthesis in AGB stars and unpublished data for weak *s*-process and neutron burst, Brad Meyer for discussions on the n-burst model and the latest data on the predictions for Ba isotopes in his neutron burst, and Alexander Heger for permission to use his model predictions. Andy Davis provided the AGB model data, and Lih-Sin The further predictions for weak *s*-process nucleosynthesis of Ba isotopes. We thank Michael Savina, an anonymous reviewer, and the associate editor Larry Nittler for their helpful and constructive reviews.

Editorial Handling—Dr. Larry Nittler

REFERENCES

Amari S., Hoppe P., Zinner E., and Lewis R. S. 1992. Interstellar SiC with unusual isotopic compositions: Grains from a supernova? *The Astrophysical Journal* 394:L43–L46.

Amari S., Lewis R. S., and Anders E. 1994. Interstellar grains in meteorites: I. Isolation of SiC, graphite, and diamond; size distributions of SiC and graphite. *Geochimica et Cosmochimica Acta* 58:459–470.

Amari S., Hoppe P., Zinner E. K., and Lewis R. S. 1995. Trace-element concentrations in single circumstellar silicon carbide grains from the Murchison meteorite. *Meteoritics* 30:679–693.

Argast D., Samland M., Thielemann F.-K., and Qian Y.-Z. 2004. Neutron star mergers versus core-collapse supernovae as dominant *r*-process sites in the early galaxy. *Astronomy & Astrophysics* 416:997–1011.

Arlandini C., Käppeler F., Wisshak K., Gallino R., Busso M., and Straniero O. 1999. Neutron capture in low-mass asymptotic giant branch stars: Cross sections and abundance signatures. *The Astrophysical Journal* 525:886–900.

Barzyk J. G., Savina M. R., Davis A. M., Gallino R., Pellin M. J., Lewis R. S., Amari S., and Clayton R. N. 2006. Multi-element isotopic analysis of single presolar SiC grains. *New Astronomy Reviews* 50:587–590.

Barzyk J. G., Savina M. R., Davis A. M., Gallino R., Gyngard F., Amari S., Zinner E., Pellin M. J., Lewis R. S., and Clayton R. N. 2007. Constraining ^{13}C amounts in AGB stars through measurement of trace elements in presolar SiC. *Meteoritics & Planetary Science* 42. This issue.

Bernatowicz T., Fraundorf G., Tang M., Anders E., Wopenka B., Zinner E., and Fraundorf P. 1987. Evidence for interstellar SiC in the Murray carbonaceous meteorite. *Nature* 330:728–730.

Besmehn A. and Hoppe P. 2001. Silicon- and calcium-isotopic compositions of presolar silicon nitride grains from the Indarch enstatite chondrite (abstract #1188). 32nd Lunar and Planetary Science Conference. CD-ROM.

Besmehn A., Mostefaoui S., and Hoppe P. 2001. Presolar minerals in the enstatite chondrite Sahara 97166 (abstract #5184). *Meteoritics & Planetary Science* 36:A20.

Boothroyd A. I., Sackmann I.-J., and Ahern S. C. 1993. Prevention of high-luminosity carbon stars by hot bottom burning. *The Astrophysical Journal* 416:762–768.

Bonacic Marinovic A., Izzard R. G., Lugaro M., and Pols O. R. 2006. Population synthesis of *s*-process element enhanced stars: Constraining the ^{13}C efficiency. *Memorie della Societa Astronomica Italiana* 77:879–884.

Burbidge E. M., Burbidge G. R., Fowler W. A., and Hoyle F. 1957. Synthesis of the elements in stars. *Review of Modern Physics* 29: 547–650.

Cameron A. G. W. 1957. Nuclear reactions in stars and nucleogenesis. *Publications of the Astronomical Society of the Pacific* 69:201–222.

Clayton D. D. 1989. Origin of heavy xenon in meteoritic diamonds. *The Astrophysical Journal* 340:613–619.

Davis A. M. 2004. The *r*-process record in meteorites. In *Proceedings from the institute for nuclear theory*, vol. 13, edited by Qian Y.-Z., Rehm E., Schatz H., and Thielemann F.-K. Singapore: World Scientific. pp. 120–128.

Frost C. A., Cannon R. C., Lattanzio J. C., Wood P. R., and Forestini M. 1998. The brightest carbon stars. *Astronomy & Astrophysics* 332:L17–L20.

Gallino R., Raiteri C. M., and Busso M. 1993. Carbon stars and isotopic Ba anomalies in meteoritic SiC grains. *The Astrophysical Journal* 410:400– 411.

Gallino R., Arlandini C., Busso M., Lugaro M., Travaglio C., Straniero O., Chieffi A., and Limongi M. 1998. Evolution and nucleosynthesis in low-mass asymptotic giant branch stars. II. Neutron capture and the *s*-process. *The Astrophysical Journal* 497:388–403.

Gao X., Nittler L. R., Swan P. D., and Walker R. M. 1995. Presolar grains in Indarch (abstract). *Meteoritics* 30:508.

Gao X., Amari S., Messenger S., Nittler L. R., Swan P. D., and Walker R. M. 1996. Survey of circumstellar grains in the unique carbonaceous chondrite Acfer 094 (abstract). *Meteoritics & Planetary Science* 31:A48.

Haas M. R., Colgan S. W. J., Erickson E. F., Lord S. D., Burton M. G., and Hollenbach D. J. 1990. Velocity-resolved far-infrared spectra of [Fe II]: Evidence for mixing and clumping in SN 1987A. *The Astrophysical Journal* 360:257–266.

Heck Ph. R., Marhas K. K., Baur H., Hoppe P., and Wieler R. 2007. Presolar He and Ne isotopes in single circumstellar SiC grains *The Astrophysical Journal* 656:1208–1222.

Heymann D. and Dziczkaniec M. 1979. Xenon from intermediate zones of supernovae. Proceedings, 10th Lunar and Planetary Science Conference. pp. 1943–1959.

Hillion F., Daigne B., Girard F., Slodzian G., and Schuhmacher M. 1994. A new high performance instrument: The Cameca "NanoSIMS 50." In *Secondary Ion Mass Spectrometry, Proceedings SIMS IX*, edited by Benninghoven A., Nihei Y., Shimizu R., and Werner H. W. Chichester: John Wiley & Sons. pp. 254–257.

Hoppe P. 2004. Stardust in meteorites. In *Astrophysics of dust*, edited by Witt A. N., Clayton G. C., and Draine B. T. San Francisco: Astronomical Society of the Pacific. pp. 265–283.

Hoppe P. and Ott U. 1997. Mainstream silicon carbide grains from meteorites. In *Astrophysical implication of the laboratory study of presolar materials,* edited by Bernatowicz T. J. and Zinner E. K. New York: American Institute of Physics. pp. 27–58.

Hoppe P. and Besmehn A. 2002. Evidence for extinct vanadium-49 in presolar silicon carbide grains from supernovae. *The Astrophysical Journal* 576:L69–L72.

Hoppe P., Strebel R., Eberhardt P., Amari S., and Lewis R. 2000. Isotopic properties of silicon carbide X grains from the Murchison meteorite in the size range 0.5–1.5 μm. *Meteoritics & Planetary Science* 35:1157–1176.

Howard W. M., Meyer B. S., and Clayton D. D. 1992. Heavy-element abundances from a neutron burst that produces Xe-H. *Meteoritics* 27:404–412.

Huss G. R. and Lewis R. S. 1994. Noble gases in presolar diamonds I: Three distinct components and their implications for diamond origins. *Meteoritics* 29:791–810.

Jennings C. L., Savina M. R., Messenger S., Amari S., Nichols R. H., Jr., Pellin M. J., and Podosek F. A. 2002. Indarch SiC by TIMS, RIMS, and NanoSIMS (abstract #1833). 33rd Lunar and Planetary Science Conference. CD-ROM.

Käppeler F., Beer H., and Wisshak K. 1989. *s*-Process nucleosynthesis—Nuclear physics and the classical model. *Reports on Progress in Physics* 52:945–1013.

Karakas A. 2003. Asymptotic giant branch stars: Their influence on binary systems and the interstellar medium. Ph.D. thesis, Monash University, Australia.

Kosaza T., Hasegawa H., and Nomoto K. 1991. Formation of dust grains in the ejecta of SN 1987A. II. *Astronomy & Astrophysics* 249:474–482.

Kratz K.-L., Bitouzet J.-P., Thielemann F.-K., Möller P., and Pfeiffer B. 1993. Isotopic *r*-process abundances and nuclear structure far from stability: Implication for the *r*-process mechanism. *The Astrophysical Journal* 403:216–238.

Lewis R. S., Srinivasan B., and Anders E. 1975. Host phase of a strange xenon component in Allende. *Science* 190:1251–1262.

Lewis R. S., Tang M., Wacker J. F., Anders E., and Steel E. 1987. Interstellar diamonds in meteorites. *Nature* 326:160–162.

Lin Y., Amari S., and Pravdivtseva O. 2002. Presolar grains from the Qinzhen (EH3) meteorite. *The Astrophysical Journal* 575:257–263.

Lodders K. and Fegley B., Jr. 1995. The origin of circumstellar silicon carbide grains found in meteorites. *Meteoritics* 30:661–678.

Lodders K. and Fegley B., Jr. 1997. Complementary trace element abundances in meteoritic SiC grains and carbon star atmospheres. *The Astrophysical Journal* 484:L71– L74.

Lugaro M., Davis A. M., Gallino R., Pellin M. J., Straniero O., and Käppeler F. 2003. Isotopic compositions of strontium, zirconium, molybdenum, and barium in single presolar SiC grains and asymptotic giant branch stars. *The Astrophysical Journal* 593:486–508.

Manuel O. K., Hennecke E. W., and Sabu D. D. 1972. Xenon in carbonaceous chondrites. *Nature* 240:99–101.

Mathews G. J., Bazan G., and Cowan J. J. 1992. Evolution of heavy-element abundances as a constraint on sites for neutron-capture nucleosynthesis. *The Astrophysical Journal* 391:719–735.

McCulloch M. T. and Wasserburg G. J. 1978. Barium and neodymium isotopic anomalies in the Allende meteorite. *The Astrophysical Journal* 220:L15–L19.

Messenger S., Keller L. P., Stadermann F. J., Walker R. M., and Zinner E. 2003. Samples of stars beyond the solar system: Silicate grains in interplanetary dust. *Science* 300:105–108.

Meyer B. S., Clayton D. D., and The L.-S. 2000. Molybdenum and zirconium isotopes from a supernova neutron burst. *The Astrophysical Journal* 540:L49–L52.

Mostefaoui S. and Hoppe P. 2004. Discovery of abundant in situ silicate and spinel grains from red giant stars in a primitive meteorite. *The Astrophysical Journal* 613:L149–L152.

Nguyen A. and Zinner E. 2004. Discovery of ancient silicate stardust in a meteorite. *Science* 303:1496–1499.

Nicolussi G. K., Davis A. M., Pellin M. J., Lewis R. S., Clayton R. N., and Amari S. 1997. *s*-Process zirconium in presolar silicon carbide grains. *Science* 277:1281–1283.

Nicolussi G. K., Pellin M. J., Lewis R. S., Davis A. M., Amari S., and Clayton R. N. 1998. Molybdenum isotopic composition of individual presolar silicon carbide grains from the Murchison meteorite. *Geochimica et Cosmochimica Acta* 62: 1093–1104.

Nittler L. R. 1996. Quantitative isotopic ratio ion imaging and its application to studies of preserved stardust in meteorites. Ph.D. thesis, Washington University, Saint Louis, Missouri, USA. 210 p.

Nittler L. R. 2003. Presolar stardust in meteorites: Recent advances and scientific frontiers. *Earth and Planetary Science Letters* 209: 259–273.

Nittler L. R., Amari S., Zinner E., Woosley S. E., and Lewis R. S. 1996. Extinct ^{44}Ti in presolar graphite and SiC: Proof of a supernova origin. *The Astrophysical Journal* 462:L31– L34.

Ott U. 1996. Interstellar diamond xenon and time scales of supernova ejecta. *The Astrophysical Journal* 463:344–348.

Ott U. 2002. Meteoritic anomalies, rapid neutron capture, and gamma-rays. *New Astronomy Review* 46:513–518.

Ott U. and Begemann F. 1990. Discovery of *s*-process barium in the Murchison meteorite. T*he Astrophysical Journal* 353:L57–L60.

Pellin M. J., Davis A. M., Lewis R. S., Amari S., and Clayton R. N. 1999. Molybdenum isotopic composition of single silicon carbide grains from supernovae (abstract #1969). 30th Lunar and Planetary Science Conference. CD-ROM.

Pellin M. J., Calaway W. F., Davis A. M., Lewis R. S., Amari S., and Clayton R. N. 2000. Toward complete isotopic analysis of individual presolar silicon carbide grains: C, N, Si, Sr, Zr, Mo, and Ba in single grains of type X (abstract #1917). 31st Lunar and Planetary Science Conference. CD-ROM.

Pellin M. J., Savina M. R., Calaway W. F., Tripa C. E., Barzyk J. G., Davis A. M., Gyngard F., Amari S., Zinner E., Lewis R. S., and Clayton R. N. 2006. Heavy metal isotopic anomalies in supernovae presolar grains (abstract #2041). 37th Lunar and Planetary Science Conference. CD-ROM.

Prombo C. A., Podosek F. A., Amari S., and Lewis R. S. 1993. *s*-Process Ba isotopic compositions in presolar SiC from the Murchison meteorite. *The Astrophysical Journal* 410:393–399.

Qian Y.-Z. 2003. The origin of the heavy elements: Recent progress in the understanding of the *r*-process. *Progress in Particle and Nuclear Physics* 50:153–199.

Qian Y.-Z. 2005 Nuclear physics and astrophysics of the *r*-process. *Nuclear Physics A* 752:550–559.

Raiteri C. M., Gallino R., Busso M., Neuberger D., and Käppeler F. 1993. The weak s-component and nucleosynthesis in massive stars. *The Astrophysical Journal* 419:207–223.

Rauscher T., Heger A., Hoffman R. D., and Woosley S. E. 2002. Nucleosynthesis in massive stars with improved nuclear and stellar physics. *The Astrophysical Journal* 576:323–348.

Reynolds J. H. 1960. Determination of the age of the elements. *Physical Review Letters* 4:8–10.

Reynolds J. H. and Turner G. 1964. Rare gases in the chondrite Renazzo. *Journal of Geophysical Research* 69:3263–3281.

Russell S. S., Ott U., Alexander C. M. O'D., Zinner E. K., Arden J. W., and Pillinger C. T. 1997. Presolar silicon carbide from the Indarch (EH4) meteorite: Comparison with silicon carbide populations from other meteorite classes. *Meteoritics & Planetary Science* 32:719–732.

Savina M. R., Davis A. M., Tripa C. E., Pellin M. J., Clayton R. N., Lewis R. S., Amari S., Gallino R., and Lugaro M. 2003. Barium isotopes in individual presolar silicon carbide grains from Murchison meteorite. *Geochimica et Cosmochimica Acta* 67: 3201–3214.

Sneden C., Cowan J. J., Ivans I. I., Fuller G. M., Burles S., Beers T. C., and Lawler J. E. 2000. Evidence of multiple *r*-process sites in the early galaxy: New observations of CS 22892–052. *The Astrophysical Journal* 533:L139–L142.

Straniero O., Gallino R., Busso M., Chieffi A., Raiteri C. M., Limongi M., and Salaris M. 1995. Radiative ^{13}C burning in asymptotic giant branch stars and *s*-processing. *The Astrophysical Journal* 440:L85–L87.

Takahashi K. and Yokoi K. 1987. Beta-decay rates of highly ionized heavy atoms in stellar interiors. *Atomic Data and Nuclear Data Tables* 36:375–409.

The L.-S., El Eid M. F., and Meyer B. S. 2007. *s*-Process nucleosynthesis in advanced burning phases of massive stars. *The Astrophysical Journal* 655:1058–1078.

Travaglio C., Galli D., Gallino R., Busso M., Ferrini F., and Straniero O. 1999. Galactic chemical evolution of heavy elements: From barium to europium. *The Astrophysical Journal* 521:691–702.

Verchovsky A. B. and Wright I. P. 2004. Physical parameters of AGB winds derived from the implanted species in meteoritic SiC grains. *Memorie della Società Astronomica Italiana* 75:623–626.

Verchovsky A. B., Wright I. P., and Pillinger C. T. 2004. Astrophysical significance of asymptotic giant branch stellar wind energies recorded in meteoritic SiC grains. *The Astrophysical Journal* 607:611–619.

Yin Q.-Z., Lee C.-T. A., and Ott U. 2006. Signatures of the *s*-process in presolar silicon carbide grains: Barium through hafnium. *The Astrophysical Journal* 647:676–684.

Zinner E. 2004. Presolar grains. In *Meteorites, comets, and planets*, edited by Davis A. M. Treatise on Geochemistry, vol.1. Oxford, San Diego: Elsevier. pp. 17–39.

Zinner E., Amari S., and Lewis R. S. 1991. *s*-Process Ba, Nd, and Sm in presolar SiC from the Murchison meteorite. *The Astrophysical Journal* 382:L47–L50.